Tectonic controls on sedimentary provenance and basin geography of the Mesoproterozoic Wilton package, McArthur Basin, northern Australia

Bo Yang[1,2] , Alan S. Collins[1,2], Morgan L. Blades[1,2], Tim J. Munson[3], Justin L. Payne[2,4], Stijn Glorie[1,2] and Juraj Farkaš[1,2]

[1]Tectonics and Earth Systems Research Group, Department of Earth Sciences, The University of Adelaide, SA 5005, Australia; [2]Mineral Exploration Cooperative Research Centre; [3]NT Geological Survey, Department of Primary Industry and Resources, GPO Box 4550, Darwin, NT 0801, Australia and [4]School of Natural and Built Environments, Mawson Lakes Campus, University of South Australia, SA 5095, Australia

Abstract

The *c.* 1.5–1.3 Ga Wilton package, the upper succession of the greater McArthur Basin, preserves detailed tectono-sedimentary evidence for the Mesoproterozoic evolution of the North Australian Craton (NAC). In addition, it is a valuable global sedimentary repository for the poorly explored Mesoproterozoic. New detrital zircon U–Pb age and Lu–Hf isotope data, collected from multiple, geographically separated, basins that make up the Wilton package, are compiled with previously published data to illuminate the basin evolution. The spatial and temporal variation in sedimentary provenance illustrates two major geographic changes that correspond to continent-scale tectonic convulsions of the NAC during the Mesoproterozoic. The first is shown by the influx of sediment sourced from east and southeast terranes. This is linked to rifting between Proterozoic Australia and Laurentia at *c.* 1.45 Ga, resulting in the uplift of the eastern margin of the NAC–SAC (South Australian Craton). The second basin geographic change is illustrated by a flux of southerly-sourced detritus that is interpreted to be tectonically driven by the uplift of the southern NAC, during the subduction/closure of the Mirning Ocean at *c.* 1.32 Ga. Spatially, sediment in the Wilton package is separated into two depositional systems: sedimentary rocks within the Birrindudu Basin, the western component of the Wilton package, have different detrital signatures relative to other Wilton package successions found east of the Daly Waters Fault Zone, in the Beetaloo Sub-basin, the McArthur Basin and the South Nicholson Basin. The Daly Waters Fault Zone is interpreted as an ancient bathymetric high, blocking sediment transport. Although they differ in sources, rocks in both the Birrindudu Basin and the eastern Wilton package record coeval shifts of basin provenance to southern sources. The coherent evolution of basin provenance indicates a consistent tectono-sedimentation history, and links the Birrindudu Basin and the other Wilton successions in a tectonic framework.

1. Introduction

The Mesoproterozoic is a relatively poorly explored interval in Earth history. This is despite considerable evidence that this time witnessed dramatic plate tectonic events that may have causal links to major biological, atmospheric and ocean chemistry changes (Javaux *et al.* 2001; Lyons *et al.* 2014; Planavsky *et al.* 2014; Sperling *et al.* 2014; Butterfield, 2015; Mukherjee *et al.* 2018; Tang *et al.* 2016; Zhu *et al.* 2016; Zhang *et al.* 2018; Allen *et al.* 2019). The *c.* 1.8–0.9 Ga greater McArthur Basin, northern Australia, is one of the largest and best-preserved global sedimentary archives of this era (Fig. 1). Sedimentary geochemical proxies from the greater McArthur successions have been used to investigate the Mesoproterozoic ocean chemistry (Shen *et al.* 2003; Cox *et al.* 2019), atmospheric compositions (Reinhard *et al.* 2013; Mukherjee & Large, 2016) and biological conditions (Mukherjee *et al.* 2018, 2019). The tectonic geography of the greater McArthur Basin, however, is still largely unknown. This is a critical gap in knowledge, because nutrient supply, from erosion of tectonically generated topography and/or volcanism, regulated local biological productivity, which subsequently influenced the basinal biochemical cycles and redox conditions (Cox *et al.* 2016; Yang *et al.* 2020). It is likely that individual basins, or even parts of basins, might have different geochemical profiles due to variable productivity that would have been controlled by the flux of nutrients. To understand these feedbacks, we must understand the evolution of the tectonic geography of the basin.
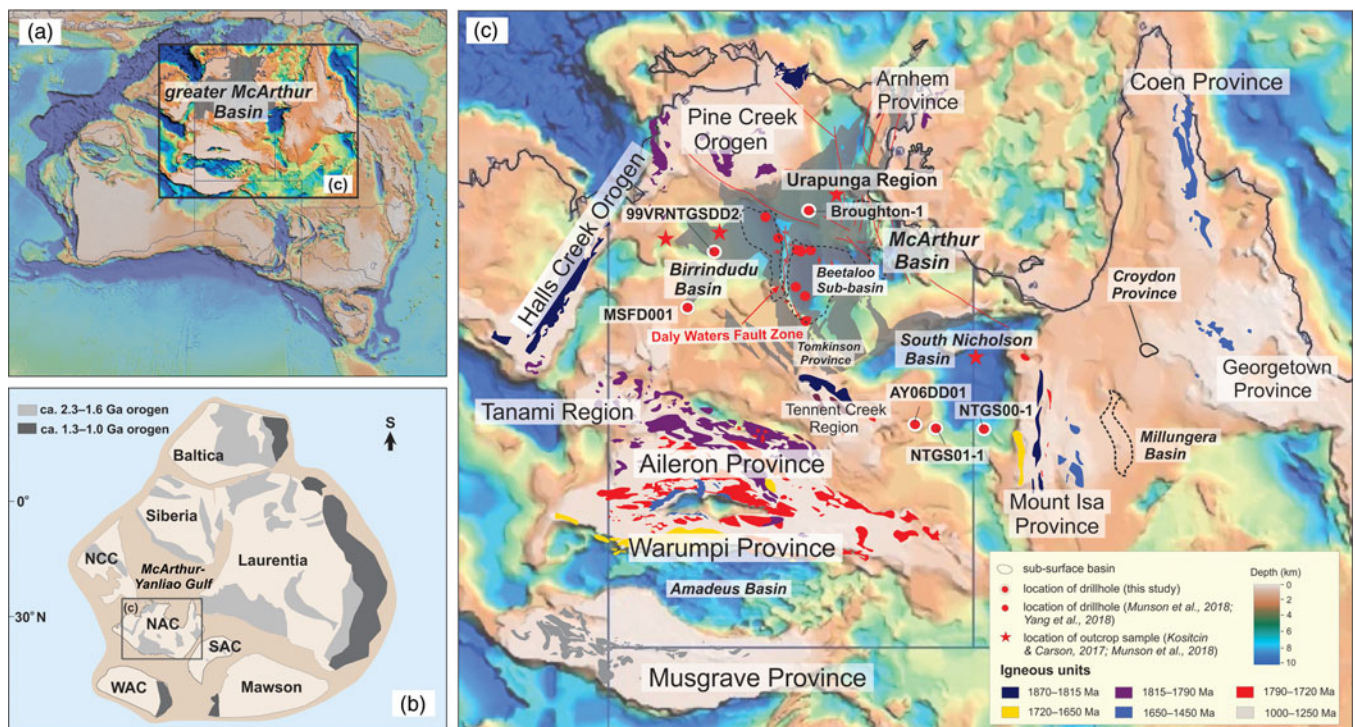
Fig. 1. (a) Top-to-basement map (SEEBASE™ basement surface image after Frogtech Geoscience, 2018), showing the location of the greater McArthur Basin and the North Australian Craton (NAC). (b) Location of the Mesoproterozoic NAC within the *c.* 1.3 Ga Rodinia Supercontinent (modified after Kirscher *et al.* 2018). (c) Tectonic framework of the NAC with the locations of interpreted Wilton package (shade area), orogens and sampled boreholes, modified after Munson (2016) and Yang *et al.* (2018).

This study attempts to address the tectonic geography of the greater McArthur Basin. This will enable future studies to better place this depositional system into a wider regional and global context, to better understand whether geochemical proxies may reflect widespread basin-wide or even global effects, or whether they better represent local productivity-driven phenomena (e.g. Cox *et al.* 2016; Yang *et al.* 2020). Here, we focus on the upper package of greater McArthur Basin (the Wilton package), and present data from samples that were collected from multiple basins whose sedimentary accumulations make up the Wilton package, including the Roper Group of the McArthur Basin, the Tijunna–Bullita groups of the Birrindudu Basin and the South Nicholson Group of the South Nicholson Basin (Fig. 1). New detrital zircon U–Pb and Lu–Hf data, compiled with previous published data, are used to determine the basin source regions and intra-basin correlations. From the interpreted spatial and temporal provenance evolution, we reconstruct the tectonic geography of northern Australia during the middle Mesoproterozoic.

2. Geological setting

The greater McArthur Basin is a regionally extensive depositional area in which Palaeoproterozoic to Mesoproterozoic rocks occur, and that covers a large area of northern Australia (Fig. 1; Rawlings, 1999; Ahmad & Munson, 2013; Close, 2014). Rocks of the basin unconformably overlie Archaean- to early Palaeoproterozoic-aged crystalline basement and are unconformably overlain by Neoproterozoic and Phanerozoic sedimentary rocks (Fig. 2). The greater McArthur Basin contains several coherent lithostratigraphic components and is subdivided into five sedimentary packages (Rawlings, 1999; Ahmad & Munson, 2013; Munson, 2016; Munson *et al.* 2018). The uppermost Wilton package is

characterized by Mesoproterozoic siliciclastic rocks that are readily distinguished from the underlying carbonate-dominated successions of the Favenc package (Fig. 2; Rawlings, 1999; Munson, 2016; Munson *et al.* 2018). The Wilton package is shown to be continuous in the subsurface, between basins, in seismic sections (Williams, 2019) and is interpreted to be preserved in several geographically widely separated basins (Munson, 2016; Frogtech Geoscience, 2018; Munson *et al.* 2018). Rocks in these basins include the Roper Group of the McArthur Basin and the buried Beetaloo Sub-basin (Williams, 2019), the Renner Group of the Tomkinson Province, the Tijunna Group of the Birrindudu Basin, and the South Nicholson Group of the South Nicholson Basin (Fig. 1; Rawlings, 1999; Close, 2014; Munson, 2016; Munson *et al.* 2018). Sedimentary rocks of the Wilton package are dominated by alternating sandstone and mudstone units and are interpreted to have been deposited in a range of depositional environments, from shoreline to shallow-marine shelf (Rawlings, 1999; Munson, 2016; Sheridan *et al.* 2018).

2.a. Roper Group

Sedimentary rocks of the Roper Group are exposed in the McArthur Basin and in the subsurface Beetaloo Sub-basin (Fig. 1; Ahmad & Munson, 2013; Munson, 2016; Williams, 2019). The Roper Group is interpreted to have been deposited in a stable shoreline–shelf environment and is subdivided into two subgroups: the lower Collara Subgroup and the upper Maiwok Subgroup (Fig. 2; Rawlings, 1999; Abbott & Sweet, 2000). The Collara Subgroup consists of eight units, dominated by sandstones, with less voluminous mudrocks. In ascending stratigraphic order, these are the Phelp Sandstone, Mantungula Formation, Limmen Sandstone, Mainoru Formation, Arnold
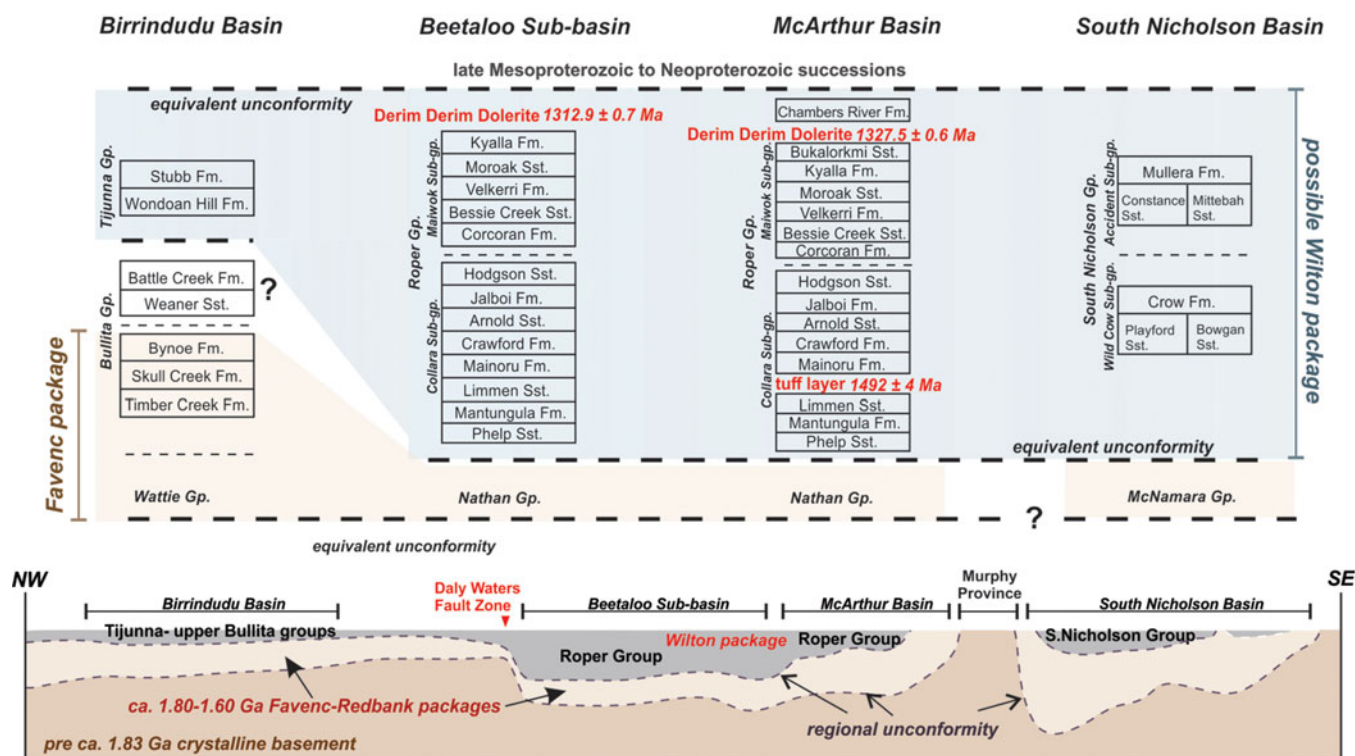
Fig. 2. Stratigraphic chart of the Wilton package and its potential equivalents, after Ahmad & Munson (2013), Munson (2016) and Munson *et al.* (2018). Diagrammatic cross-section showing the stratigraphy of the Wilton package, modified after Frogtech Geoscience (2018). Note that the top of the Wilton package has been normalized to surface. Not to scale. Gp: Group; Sub-gp: Subgroup. Dolerite baddeleyite isotope dilution thermal ionization mass spectrometry (ID-TIMS) ages are from Yang *et al.* (2020) and Bodorkos *et al.* (2020).

Sandstone, Jalboi Formation and Hodgson Sandstone (Fig. 2; Jackson *et al.* 1988; Rawlings, 1999; Abbott & Sweet, 2000; Abbott *et al.* 2001; Munson, 2016). The Maiwok Subgroup is more mudrock-rich with less abundant sandstones; finer-grained units are interpreted as having been deposited in slightly deeper shelf environments (Munson, 2016 and references therein). Seven sedimentary units are included in this subgroup: in ascending stratigraphic order these are the Corcoran Formation, Bessie Creek Sandstone, Velkerri Formation, Moroak Sandstone, Kyalla Formation, the Bukalorkmi Sandstone and Chambers River Formation (Fig. 2; Ahmad & Munson, 2013). The Chambers River Formation has an isolated distribution, north of the Beetaloo Sub-basin, and is currently under review for promotion to status as a group (TJ Munson & B Yang, pers. comm.). A sensitive high-resolution ion microprobe (SHRIMP) U–Pb zircon age of 1492 ± 4 Ma (2σ; Jackson *et al.* 1999), from a tuffaceous bed within the lower Mainoru Formation, provides a maximum depositional age constraint on the Collara Subgroup (Fig. 2). The youngest single grain age of 1386 ± 13 Ma from the Bessie Creek Sandstone has been used as the maximum depositional age constraint for the Maiwok Subgroup (Yang *et al.* 2018). The minimum depositional age of the Roper Group is constrained by the age of the Derim Derim Dolerite that intrudes the upper part of the succession up to the Bukalorkmi Sandstone (Fig. 2). A secondary ionization mass spectrometry (SIMS) U–Pb baddeleyite age of 1324 ± 4 Ma, was reported by Abbott *et al.* (2001) from the Urapunga Region for the Derim Derim Dolerite. This has recently been confirmed with an isotope dilution thermal ionization mass spectrometry (ID-TIMS) age of 1327.5 ± 0.6 Ma (Bodorkos *et al.* 2020) on the same baddeleyite sample. Yang *et al.* (2020) obtained

a younger ID-TIMS U–Pb baddeleyite age of 1312.9 ± 0.9 Ma from a sample of the dolerite collected from the northern Beetaloo Sub-basin *c.* 200 km south of the Urapunga Region.

2.b. Bullita and Tijunna groups

The Birrindudu Basin is located in the western part of the greater McArthur Basin (Figs 1, 2). The two uppermost sedimentary groups are the Bullita and Tijunna groups (Fig. 2). The Bullita Group unconformably underlies the Tijunna Group, and contains five formations: in ascending stratigraphic order, the Timber Creek Formation, Skull Creek Formation, Bynoe Formation, Weaner Sandstone and Battle Creek Formation (Fig. 2; Ahmad & Munson, 2013). The three lower formations, are characterized by stromatolitic, carbonate-dominated successions, whereas the Weaner Sandstone and Battle Creek Formation contain more siliciclastics (Ahmad & Munson, 2013). Collectively, this succession indicates a shoaling, shallow-marine platform depositional environment (Ahmad & Munson, 2013). The correlation of the Bullita Group with the greater McArthur Basin packages (*sensu* Rawlings, 1999) remains unclear, as the lower formations exhibit lithological similarities to the Favenc package, whereas the siliciclastic upper formations (Weaner Sandstone and Battle Creek Formation) may correlate with the lower Wilton package (Fig. 2; Munson *et al.* 2018). Depositional age constraints for this group are limited. The youngest detrital zircon age from the underlying Wattie Group of 1550 ± 48 Ma (2σ; Kositcin & Carson, 2017) provides a maximum depositional age constraint for the lower Bullita Group formations. The maximum depositional ages of the Weaner Sandstone and the Battle Creek Formation are

constrained by the youngest single zircon analysed from the Weaner Sandstone (1550 ± 36 Ma, 2σ; Kositcin & Carson, 2017).

The Tijunna Group contains siliciclastic rocks that are divided into two formations: the Wondoan Hill Formation and the Stubb Formation (Fig. 2; Ahmad & Munson, 2013). The Wondoan Hill Formation comprises interbedded sandstone and mudstone with minor dolostone, whereas the Stubb Formation is a mudstone-dominated succession with minor sandstone. The youngest analysed detrital zircon in the Wondoan Hill Formation has a $^{207}Pb/^{206}Pb$ age of 1452 ± 48 Ma (Munson *et al.* 2018), which provides a maximum depositional age constraint. The Tijunna Group is unconformably overlain by the Neoproterozoic Auvergne Group (Carson, 2013; Munson *et al.* 2018).

2.c. South Nicholson group

The Mesoproterozoic South Nicholson Group occurs within the South Nicholson Basin, which is located to the SE of the Beetaloo Sub-basin (Figs 1, 2). This basin unconformably overlies the Palaeoproterozoic Murphy Province, Lawn Hill Platform and Western Fold Belt of the Mount Isa Province, and is overlain by a series of Neoproterozoic to Phanerozoic successions, including Cambrian volcanic rocks of the Kalkarindji Province and the Neoproterozoic Georgina Basin (Ahmad & Munson, 2013). The South Nicholson Group is dominated by quartz arenite interstratified with siltstone and shale, indicating a range of depositional environments from fluvial to shallow-marine shelf (Ahmad & Munson, 2013). It is subdivided into two subgroups. The Wild Cow Subgroup, in the lower part, includes the basal Playford Sandstone and equivalent Bowgan Sandstone, overlain by the finer-grained heterolithic Crow Formation (Fig. 2). The upper, Accident Subgroup, contains the basal Constance Sandstone and equivalent Mittebah Sandstone, overlain by the dominantly fine-grained Mullera Formation (Fig. 2). Deposition of the South Nicholson Group is constrained by a weighted mean detrital zircon age of 1483 ± 12 Ma (youngest group, 95 % confidence, *n* = 43, MSWD = 1.38) from the Crow Formation, whilst the youngest analysed zircon grain from this formation returned a $^{207}Pb/^{206}Pb$ age of 1371 ± 94 Ma (2σ; Kositcin & Carson, 2019).

3. Detrital zircon U–Pb age and Hf isotopes

3.a. Method

3.a.1. U–Pb dating

Twelve sandstones were collected from boreholes, including two from the Roper Group of the McArthur Basin, three from undifferentiated South Nicholson Group of the South Nicholson Basin, three from the Bullita Group and four from the Tijunna Group of the Birrindudu Basin. Detailed sampling information is listed in Table 1.

Zircon grains were separated from crushed rock using hand panning, conventional magnetic methods and heavy liquids (LST 2.85 ± 0.02 g mL^{-1}). Individual zircon grains were hand-picked and mounted in epoxy resin. Preference to grain sizes, or shapes, or colours was avoided during zircon selection. Cathodoluminescence (CL) images were obtained using a FEI Quanta 600 scanning electron microscope (SEM) with attached Gatan CL (working distance 15 mm; accelerating voltage 12 kV) at Adelaide Microscopy, The University of Adelaide, to image zircon internal structures and determine suitable domains for further analysis. Zircon U–Pb geochronological data were collected using a New Wave 213 nm Nd-YAG laser coupled with an Agilent 7900cs inductively coupled plasma – mass spectrometer (ICP-MS) at

Adelaide Microscopy. A spot size of 30 μm with frequency of 5 Hz was used. Laser intensity was set to 70 %, with fluence varying from ~5 to 7 J cm^{-2}. Mass bias and laser-induced fractionation were corrected using the GEMOC GJ-1 zircon standard with published $^{207}Pb/^{206}Pb$ age of 607.7 ± 4.3 Ma, $^{206}Pb/^{238}U$ age of 600.7 ± 1.1 Ma and $^{207}Pb/^{235}U$ age of 602.0 ± 1.0 Ma (Jackson *et al.* 2004).

The Plešovice and 91500 zircon standards were analysed as unknowns to check accuracy. Analysis of the Plešovice internal standard yielded a weighted average $^{206}Pb/^{238}U$ age of 336.49 ± 0.35 Ma (95 % confidence, MSWD = 1.4, *n* = 133), which is consistent with the published $^{206}Pb/^{238}U$ age of 337.13 ± 0.37 Ma (Sláma *et al.* 2008). The 91500 zircon standard yielded a $^{206}Pb/^{238}U$ weighted mean age of 1063.3 ± 4.8 Ma (95 % confidence, MSWD = 1.7, *n* = 34) and $^{207}Pb/^{206}Pb$ weighted mean age of 1064 ± 16 Ma (95 % confidence, MSWD = 1.06, *n* = 34), consistent with the published $^{206}Pb/^{238}U$ and $^{207}Pb/^{206}Pb$ ages of 1062.4 ± 0.4 Ma and 1065.4 ± 0.3 Ma (Wiedenbeck *et al.* 1995). Zircon U–Pb age concordance was calculated by dividing the $^{206}Pb/^{238}U$ age by the $^{207}Pb/^{206}Pb$ age and multiplying by 100. Data were reduced using Iolite (Paton *et al.* 2011) and plotted using the IsoplotR (Vermeesch, 2018).

3.a.2. Hafnium isotope analysis

Hafnium isotopic compositions were determined at The University of Adelaide using a New Wave UP-193 ArF excimer laser attached to a Thermo-Scientific Neptune Multi-Collector ICP-MS, following the methodology of Payne *et al.* (2013). Zircon grains, with less than 10 % age discordance, were ablated using a spot size of 50 μm or 35 μm (depending on the grain size), frequency of 5 Hz, 4 ns pulse length and an intensity of ~4.5 J cm^{-2}. The acquisition time of each analysis was ~70 s, including 20 s of gas background measurement. Raw data were reduced using the HfTRAX Excel macro (Payne *et al.* 2013). Hafnium mass bias was corrected using a stable $^{179}Hf/^{177}Hf$ ratio of 0.7325 (Patchett *et al.* 1982). Correction of the Yb and Lu isobaric interferences on ^{176}Hf followed the methods of Woodhead *et al.* (2004). The Mudtank zircon standard was used to monitor the instrument stability and data quality. This yielded a weighted mean $^{176}Hf/^{177}Hf$ ratio of 0.282499 ± 14 (2σ, *n* = 10), which is in accordance with the published value of 0.282507 ± 6 (Woodhead & Hergt, 2005). A ^{176}Lu decay constant of 1.865 × 10^{-11} a^{-1} after Scherer *et al.* (2001) was used for initial $^{176}Hf/^{177}Hf$ values calculation. ε$_{Hf}$(*t*) values were calculated using chondrite reservoir (CHUR) values of $^{176}Hf/^{177}Hf$ = 0.282785 and $^{176}Lu/^{177}Hf$ = 0.0336 after Bouvier *et al.* (2008).

3.a.3. Multidimensional scaling

We used multidimensional scaling (MDS) in this study. MDS is a statistical technique based on the Kolgomorov–Smirnov calculation (K-S test) that quantifies and visualizes the degree of dissimilarity among geochronologic samples (Vermeesch, 2013; Sharman *et al.* 2018). The degree of dissimilarity is visualized by the plotted distance between individual samples. Samples that have similar age spectra plot closer to each other than samples that have less similar spectra. Although limitations exist (e.g. Yang *et al.* 2018; Nordsvan *et al.* 2020), the MDS plot presents a useful comparison of samples from various locations and stratigraphy, providing assessments on both spatial and temporal variation of basin provenance. In this study, the MDS plot was generated using detritalPy (Sharman *et al.* 2018), with individual samples presented as pie charts for the purpose of illustrating the detrital zircon age compositions for each sample. Data from potential sourcing basements were also

Table 1. Details of samples collected for this study

Basin	Borehole	Coordinate	Sample	Group	Formation	Lithology
McArthur Basin	Broughton-1	E: 133.62607°	Bro-07	Collara Sub-gp.	Arnold Sst.	coarse-grained sandstone
		S: −14.35995°	Bro-06	Collara Sub-gp.	Crawford Fm.	fine–medium-grained sandstone
Birrindudu Basin	99VRNTGSDD2	E: 131.38248°	D57	Tijunna Gp	Wondoan Hill Fm.	medium-grained sandstone
		S: −16.04131°	D24	Bullita Gp	Weaner Sst.	coarse-grained sandstone
			D02	Bullita Gp	Bynoe Fm.	fine-grained sandstone/siltstone
	MSFD001	E: 130.44231°	MS-03	Tijunna Gp	Stubb Fm.	medium-grained sandstone
		S: −17.04630°	MS-05	Tijunna Gp	Wondoan Hill Fm.	fine–medium-grained sandstone
			MS-06	Bullita Gp	Battle Creek Sst.	medium-grained sandstone
			MS-09	Bullita Gp	Weaner Sst.	coarse-grained sandstone
South Nicholson Basin	AY06DD01	E: 136.30152°	AY-01	South Nicholson Gp	undifferentiated	coarse-grained sandstone
		S: −19.83585°				
	NTGS00-1	E: 136.82621°	SOU-01	South Nicholson Gp	undifferentiated	coarse-grained sandstone
		S: −19.85399°				
	NTGS01-1	E: 137.62108°	JR-01	South Nicholson Gp	undifferentiated	coarse-grained sandstone
		S: −19.85684°				

Gp: Group; Fm: Formation; Sst: Sandstone.

plotted, highlighting variations in source regions for different parts of the basin and at different times.

3.b. Results

A total of 615 detrital zircon near-concordant (≥90 % concordance) U–Pb analyses and 253 hafnium isotope analyses were collected. All U–Pb age and hafnium value data are reported at the 2σ level. The U–Pb age data are presented in Figures 3, 4 and 5, and the hafnium data are presented in Figures 6, 7 and 8. The summarized results are provided in Table 2, and detailed analysing results are listed in the Supplementary Material available online at https://doi.org/10.1017/S0016756820001223.

Two samples from the Collara Subgroup were analysed. The Crawford Formation (Bro-06) yielded 88 near-concordant analyses (out of 142) with a dominant cluster at *c.* 1780 Ma ($\varepsilon_{Hf}(t)$: −2.9 to −0.4; Figs 3, 6). Fifty-three near-concordant (out of 107) analyses obtained from sample Bro-07 (Arnold Sandstone) exhibit a major peak at *c.* 1745 Ma ($\varepsilon_{Hf}(t)$: −4.6 to +4.4) and two minor peaks clustering at *c.* 1810 Ma ($\varepsilon_{Hf}(t)$: −5.6 to −0.4) and *c.* 1895 Ma ($\varepsilon_{Hf}(t)$: −2.6 to +0.1; Figs 3, 6).

Four samples from the Bullita Group were analysed. A total of 48 (out of 98) near-concordant analyses from the Bynoe Formation sample (D02) exhibit a major peak at *c.* 1835 Ma ($\varepsilon_{Hf}(t)$: −8.7 to +0.2) and two minor peaks at *c.* 1920 Ma ($\varepsilon_{Hf}(t)$: −4.8 to +0.2) and 1780 Ma ($\varepsilon_{Hf}(t)$: −6.8 to −5.2; Figs 4, 7). Samples D24 and MS-09 are both from the Weaner Sandstone. A total of 23 near-concordant analyses (out of 109) from sample D24 show a major age peak at *c.* 1830 Ma ($\varepsilon_{Hf}(t)$: −9.0 to +3.2) and two minor peaks at *c.* 1940 Ma ($\varepsilon_{Hf}(t)$: −6.1 to +1.7) and *c.* 1730 Ma ($\varepsilon_{Hf}(t)$: −3.7 to −0.7; Figs 4, 7). Sample MS-09 yielded 44 near-concordant analyses (out of 102) with a main and a minor peaks at *c.* 1830 Ma ($\varepsilon_{Hf}(t)$: −4.4 to +2.6) and *c.* 1910 Ma ($\varepsilon_{Hf}(t)$: −13.0 to −3.2), respectively (Figs 4, 7). The Battle Creek sample (MS-06) gave 41 near-concordant analyses (out of 124) that form an age spectrum

with a dominant age cluster at *c.* 1810 Ma ($\varepsilon_{Hf}(t)$: −6.1 to +2.1; Figs 4, 7).

Three samples from the Tijunna Group were analysed, including two from the Wondoan Hill Formation (D57 and MS-05) and one from the Stubb Formation (MS-03). Sample D57 gave 46 near-concordant analyses out of 109. These analyses exhibit a major age peak at *c.* 1795 Ma and a smaller one at *c.* 1840 Ma with $\varepsilon_{Hf}(t)$ values ranging from −4.1 to +2.6 and −3.8 to +2.5, respectively (Figs 4, 7). Sample MS-05 yielded 53 near-concordant analyses (out of 118) with a dominant age cluster at *c.* 1795 Ma ($\varepsilon_{Hf}(t)$: −6.8 to −0.2; Figs 4, 7). Forty-nine near-concordant analyses (out of 133) obtained from the Stubb Formation sample (MS-03) form a major cluster at *c.* 1810 Ma ($\varepsilon_{Hf}(t)$: −4.3 to +1.7; Figs 4, 7).

Samples AY-01, SOU-01 and JR-01 are all from the undifferentiated South Nicholson Group. Sample AY-01 gave 73 near-concordant analyses (out of 122) with a major peak at *c.* 1715 Ma ($\varepsilon_{Hf}(t)$: −5.3 to −2.2) and a minor peak at *c.* 1810 Ma ($\varepsilon_{Hf}(t)$: −6.1 to −0.5; Figs 5, 8). A total of 53 near-concordant analyses (out of 86) obtained from sample SOU-01 show one major peak and one minor peak at *c.* 1760 Ma ($\varepsilon_{Hf}(t)$: −6.9 to −1.3) and *c.* 1600 Ma ($\varepsilon_{Hf}(t)$: 463.0 to +0.5), respectively (Figs 5, 8). Sample JR-01 yielded 46 near-concordant analyses (out of 121) that form an age spectrum with a dominant peak at *c.* 1770 Ma ($\varepsilon_{Hf}(t)$: −6.3 to −2.7; Figs 5, 8).

4. Provenance analysis

The Wilton package was deposited in a stable shelf environment. It is surrounded by exposed basement that may have provided detritus to the basin at different times. In this study, coupled detrital zircon U–Pb and Hf data from the Wilton package are compared with data from the exposed orogens/basements, in order to identify the possible source regions. We recognize that none of samples here have the number of near-concordant U–Pb analyses (>117) that is
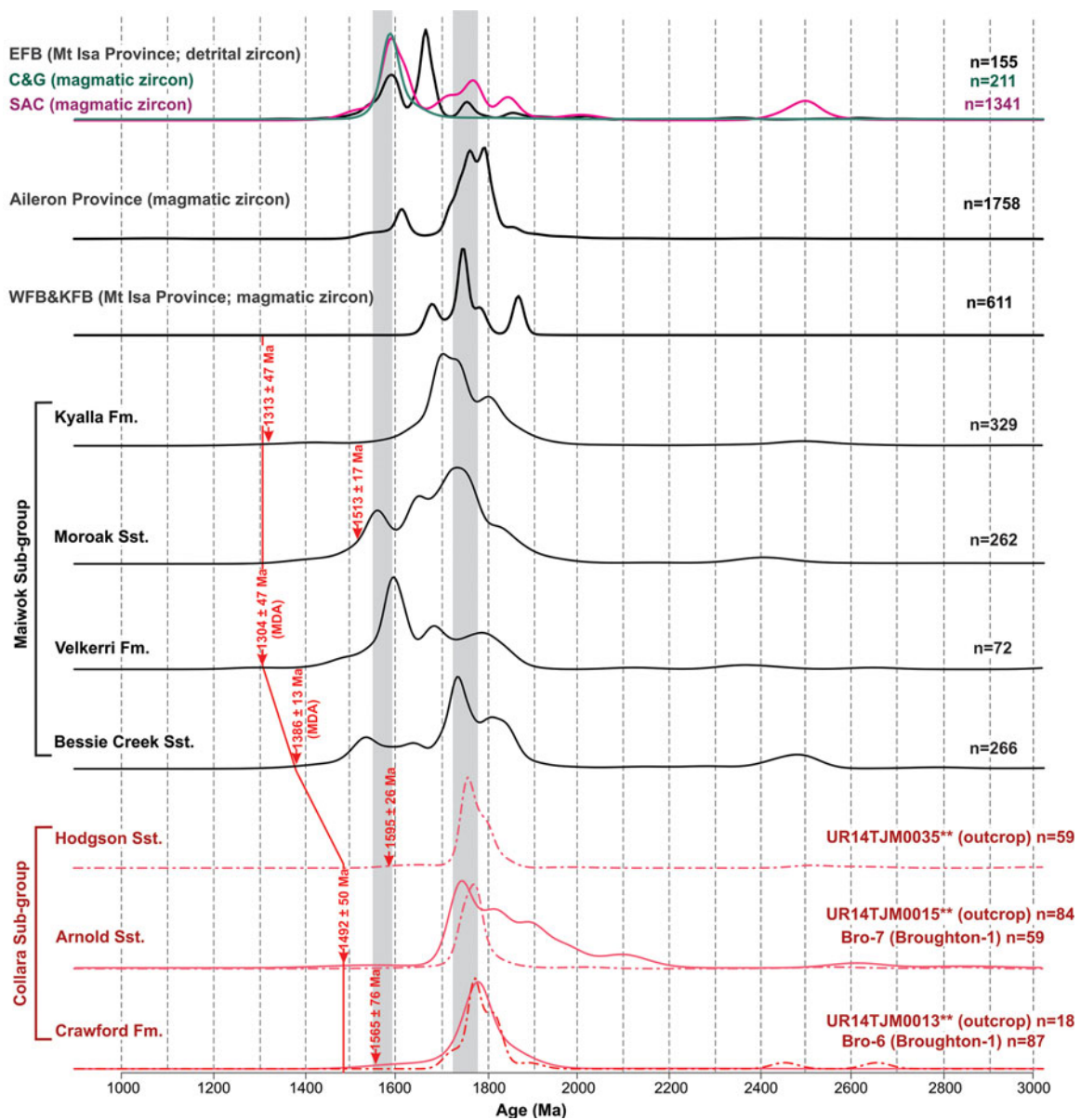
Fig. 3. Epsilon hafnium values against $^{207}Pb/^{206}Pb$ ages plot of the measured samples from the Collara Subgroup. Zircon $\epsilon_{Hf}(t)$ heat maps reflect the point density distribution of published magmatic zircon data from possible source regions, including (a) South Australian Craton (SAC; Nebel *et al.* 2007; Reid *et al.* 2008, 2014, 2017, 2020; Howard *et al.* 2009, 2011; Kromkhun *et al.* 2013; Reid & Payne, 2017), (b) Aileron Province (Hollis *et al.* 2010; Beyer *et al.* 2013, 2015) and (c) the Kathleen Fold Belt (KFB) of Mount Isa Province (Bierlein *et al.* 2008). Published detrital zircon data from source regions are from Eastern Fold Belt (EFB) of Mount Isa Province (Griffin *et al.* 2006), Coen and Georgetown provinces (C&G; Murgulov *et al.* 2007). CHUR: chondrite reservoir. *data from Munson *et al.* (2018). Maiwok Subgroup data are from Yang *et al.* (2019).

needed to record ages from all significant source regions (Vermeesch, 2004). We also recognize that sediment transport and mineral separation is not a random process. Both these caveats mean that caution is needed when interpreting gaps in data. Because of this, we have concentrated on interpreted data trends, which we argue are robust in this type of analysis. Provenance interpretations are based on the compiled new and published dataset, in order to minimize any possible statistical inaccuracy. In the kernel density plots (Figs 3, 4, 5), individual samples from the same formation are plotted separately, so that a comparison between samples can be made. Overlapping dominant age peaks from multiple samples represent the most significant age sources for each formation.

4.a. Collara Subgroup of McArthur Basin

Detrital zircon data from the sandstones in the upper part of the Collara Subgroup were derived from two core samples (Bro-06 and Bro-07; Table 1) and three outcrop samples studied by Munson *et al.* (2018); this includes sample UR14TJM0013 from the Crawford Formation, UR14TJM0015 from the Arnold Sandstone and UR14TJM0035 from the Hodgson Sandstone (Fig. 3).

The two detrital zircon spectra from the Crawford Formation, samples Bro-06 and UR14TJM0013, are unimodal, with overlapping major peaks at *c.* 1780 Ma (Fig. 3). The Arnold Sandstone spectra (Bro-07 and UR14TJM0035) are dominated by zircons
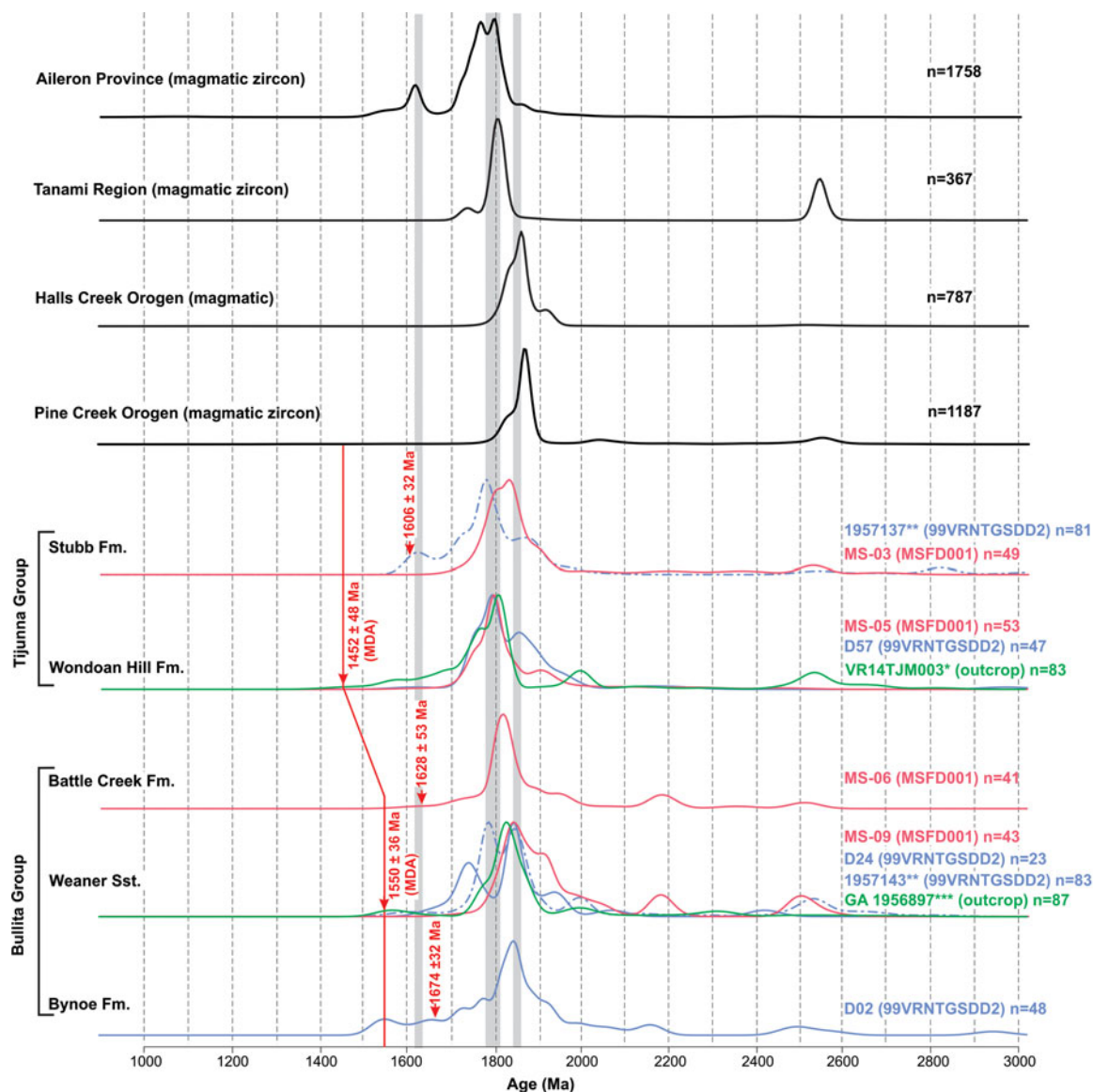
Fig. 4. Kernel distribution estimates (KDE) of detrital zircon ^{207}Pb/^{206}Pb age spectra of the Bullita and Tijunna Groups and potential sources. Data from this study are compiled with published ^{207}Pb/^{206}Pb age data from *Munson *et al.* (2018), **Carson (2013) and ***Kositcin & Carson (2017). Published ^{207}Pb/^{206}Pb ages from magmatic zircon grains are included from potential source areas, including Aileron Province (Cross *et al.* 2005*a*, *b*, *c*; Carson *et al.* 2009; Beyer *et al.* 2013, 2015, 2016; Kositcin *et al.* 2013*a*, *b*, 2014*a*, *b*, 2015; Bodorkos *et al.* 2013; Worden *et al.* 2006*a*, *b*, 2008; Hollis *et al.* 2010), Pine Creek Orogen (Carson *et al.* 2009; Kositcin *et al.* 2013*b*; Beyer *et al.* 2013; Worden *et al.* 2006*a*, *b*, 2008), Halls Creek Orogen (Worden *et al.* 2008), Tanami Region (Cross *et al.* 2005*c*; Worden *et al.* 2006*a*, 2008; Bagas *et al.* 2010; Kositcin *et al.* 2013*a*; Iaccheri, 2019). Red arrows: the youngest detrital zircon ^{207}Pb/^{206}Pb age (with >95% concordance) for each formation. MDA: the youngest detrital zircon ^{207}Pb/^{206}Pb age used as maximum deposition age constraint. Red line represents the assigned maximum deposition age for each formation. Grey columns are bands of equivalent age range.

with ^{207}Pb/^{206}Pb ages between *c.* 1800 and 1720 Ma. Major peaks are at *c.* 1780 Ma and *c.* 1745 Ma (Fig. 3). The Hodgson Sandstone sample has a unimodal spectrum with the centroid at *c.* 1760 Ma, consistent with the spectra from older sandstone units within the Collara Subgroup (Fig. 3; Munson *et al.* 2018). Although these samples all have limited concordant analyses, the similarity of these spectra to one another indicates that the sediments of these three Collara Subgroup formations were derived from similar-aged source areas. Zircon grains that form the dominant peaks at *c.* 1780 to 1740 Ma are interpreted to be sourced from *c.* 1790 to 1720 Ma magmatic rocks found in both the Mount Isa and Aileron provinces (Fig. 3). This conclusion is supported by the hafnium isotope data, which show that $\varepsilon_{Hf}(t)$ values of the Collara Subgroup overlap with those of both the

Mount Isa and Aileron provinces (Fig. 6); the similarities with the Aileron Province data are particularly striking. Sample Bro-07 also has a large portion of detrital zircon grains with ages ranging between *c.* 2150 and *c.* 1810 Ma (Fig. 3); metasedimentary rocks in Mount Isa include zircons of these ages (Fig. 6c) with similar $\varepsilon_{Hf}(t)$ values, although an additional source for these grains cannot be discounted.

4.b. Bullita and Tijunna groups of Birrindudu Basin

4.b.1. Bullita group
Detrital zircon data from three formations of the Bullita Group (Bynoe Formation, Weaner Sandstone and Battle Creek Sandstone) were derived from four new core samples (D02, D24,
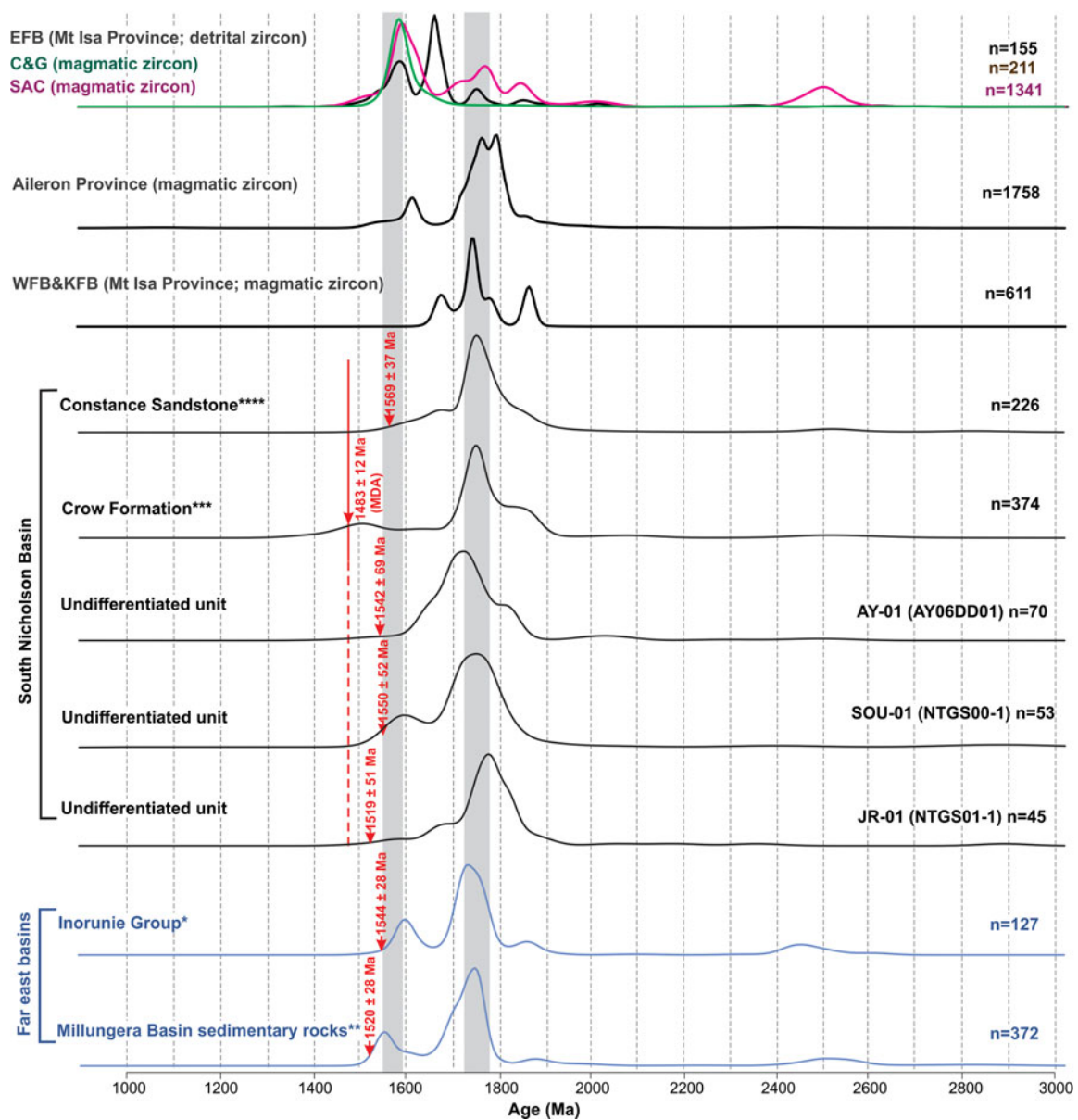
Fig. 5. Kernel distribution estimates (KDE) of detrital zircon ^{207}Pb/^{206}Pb age spectra of the South Nicholson Group, possible Wilton package equivalents and potential sources. Data used for comparison are from this study and from *Nordsvan *et al.* (2018), **Neumann & Kositcin (2011), ***Kositcin & Carson (2019) and ****Anderson *et al.* (2019). Published ^{207}Pb/^{206}Pb ages from both magmatic and detrital zircon grains are included from potential source areas, including Aileron Province (Cross *et al.* 2005*a*, *b*, *c*; Worden *et al.* 2006*a*, *b*, 2008; Carson *et al.* 2009; Hollis *et al.* 2010; Beyer *et al.* 2013, 2015, 2016; Bodorkos *et al.* 2013; Kositcin *et al.* 2013*a*, *b*, 2014*a*, *b*, 2015), Western Fold Belt & Kathleen Fold Belt (WFB&KFB) of Mount Isa Province (Neumann *et al.* 2006, 2009; Cross *et al.* 2015), Eastern Fold Belt (EFB) of Mount Isa Province (Griffin *et al.* 2006), South Australian Craton (SAC; Nebel *et al.* 2007; Reid *et al.* 2008, 2014, 2017, 2020; Howard *et al.* 2009, 2011; Wade *et al.* 2012; Kromkhun *et al.* 2013; Reid & Payne, 2017; Morrissey *et al.* 2019), Coen and Georgetown provinces (C&G; Blewett *et al.* 1998; Hoskin & Black, 2000; Kositcin *et al.* 2009; Neumann & Kositcin, 2011). Red arrows: the youngest detrital zircon ^{207}Pb/^{206}Pb age (with >95 % concordance) for each formation. MDA: the youngest detrital zircon ^{207}Pb/^{206}Pb age used as maximum deposition age constraint. Red line represents the assigned maximum deposition age for each formation. Grey columns are bands of equivalent age range.

MS-09 and MS-06; Table 1), one core sample (GA 1957143) of the Weaner Sandstone from Carson (2013) and one outcrop sample (GA 1956897) of the Weaner Sandstone from Kositcin & Carson (2017).

Only one sample (D02) was obtained from the Bynoe Formation. The age spectrum of this sample exhibits a spread of zircon ages from *c.* 2960 Ma to *c.* 1500 Ma, with a dominant age peak at 1830 Ma and minor peaks at *c.* 1920 Ma and 1780 Ma (Fig. 4). Zircon forming the prominent age peak at *c.* 1830 Ma might have been sourced from the Halls Creek and Pine

Creek orogens in the northwest and north of the basin, where voluminous *c.* 1850–1820 Ma magmatic rocks occur (Fig. 4). The minor *c.* 1920 Ma age peak also matches a similar minor peak in the Halls Creek Orogen spectrum (Fig. 4).

Age spectra from the four Weaner Sandstone samples all have primary peaks at *c.* 1830 Ma, but their secondary age populations differ (Fig. 4). These minor peaks are at *c.* 1735 Ma (sample D24), *c.* 1780 Ma (sample 1957143) and *c.* 1905 Ma (sample MS-09; Fig. 4). The differences in the minor peaks between samples may represent differences in spatial
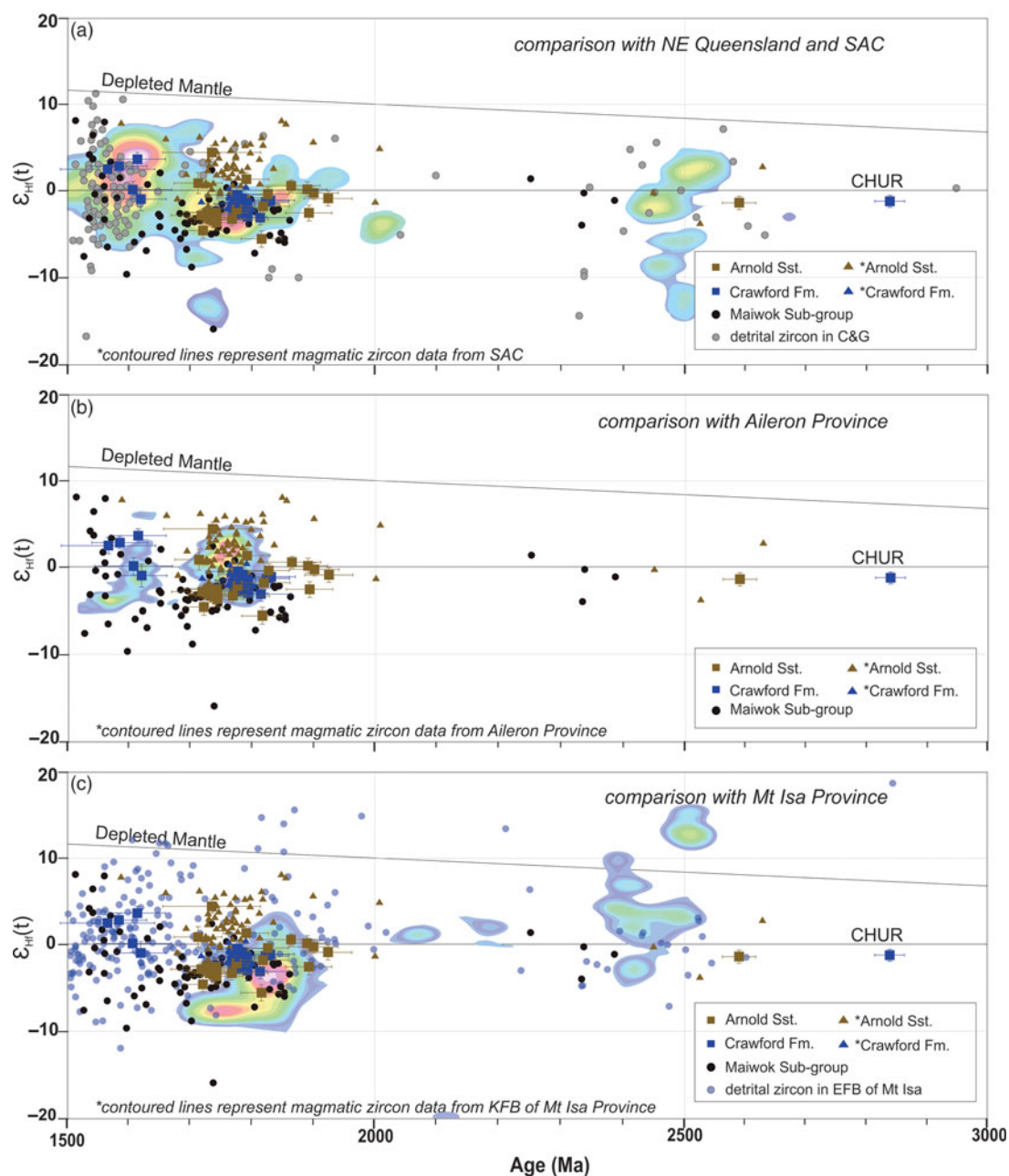
Fig. 6. Epsilon hafnium values against $^{207}Pb/^{206}Pb$ ages plot of the measured samples from the Collera Subgroup. Zircon $\epsilon_{Hf}(t)$ heat maps reflect the point density distribution of published magmatic zircon data from possible source regions, including (a) South Australian Craton (SAC; Nebel *et al.* 2007; Reid *et al.* 2008, 2014, 2017, 2020; Howard *et al.* 2009, 2011; Kromkhun *et al.* 2013; Reid & Payne, 2017), (b) Aileron Province (Hollis *et al.* 2010; Beyer *et al.* 2013, 2015) and (c) the Kathleen Fold Belt (KFB) of Mount Isa Province (Bierlein *et al.* 2008). Published detrital zircon data from source regions are from the Eastern Fold Belt (EFB) of Mount Isa Province (Griffin *et al.* 2006), the Coen and Georgetown provinces (C&G; Murgulov *et al.* 2007). CHUR: chondrite reservoir. *data from Munson *et al.* (2018). Maiwok Subgroup data are from Yang *et al.* (2019).

provenance, or simply reflect the fact that not enough zircons were analysed. Despite this, the overlapping primary *c.* 1830 Ma age peaks suggest a dominant source area, most likely the Halls Creek and Pine Creek orogens, similar to the source of the underlying Bynoe Formation. The $\epsilon_{Hf}(t)$ data show that these *c.* 1830 Ma zircon grains have $\epsilon_{Hf}(t)$ values (−9 to +3) consistent with this proposed Halls Creek/Pine Creek orogen source (Fig. 7). The *c.* 1905 Ma zircon age population is also replicated in detrital zircons from magmatic rocks in the Halls Creek / Pine Creek Orogen, but younger zircons

(<*c.* 1780 Ma) were more likely sourced from the other regions, such as the Aileron Province in the south or other unexposed sources.

Detrital zircon grains obtained from the Battle Creek Formation sample (MS-06) yielded an age spectrum with a major peak at *c.* 1810 Ma (Fig. 4). The Halls Creek and Pine Creek orogens to the north and northwest are again potential source regions for these zircons. However, there are also *c.* 1810 Ma magmatic rocks in the Tanami Region to the south of the basin. In the $\epsilon_{Hf}(t)$ vs age plot (Fig. 7c), the Battle Creek Formation analyses
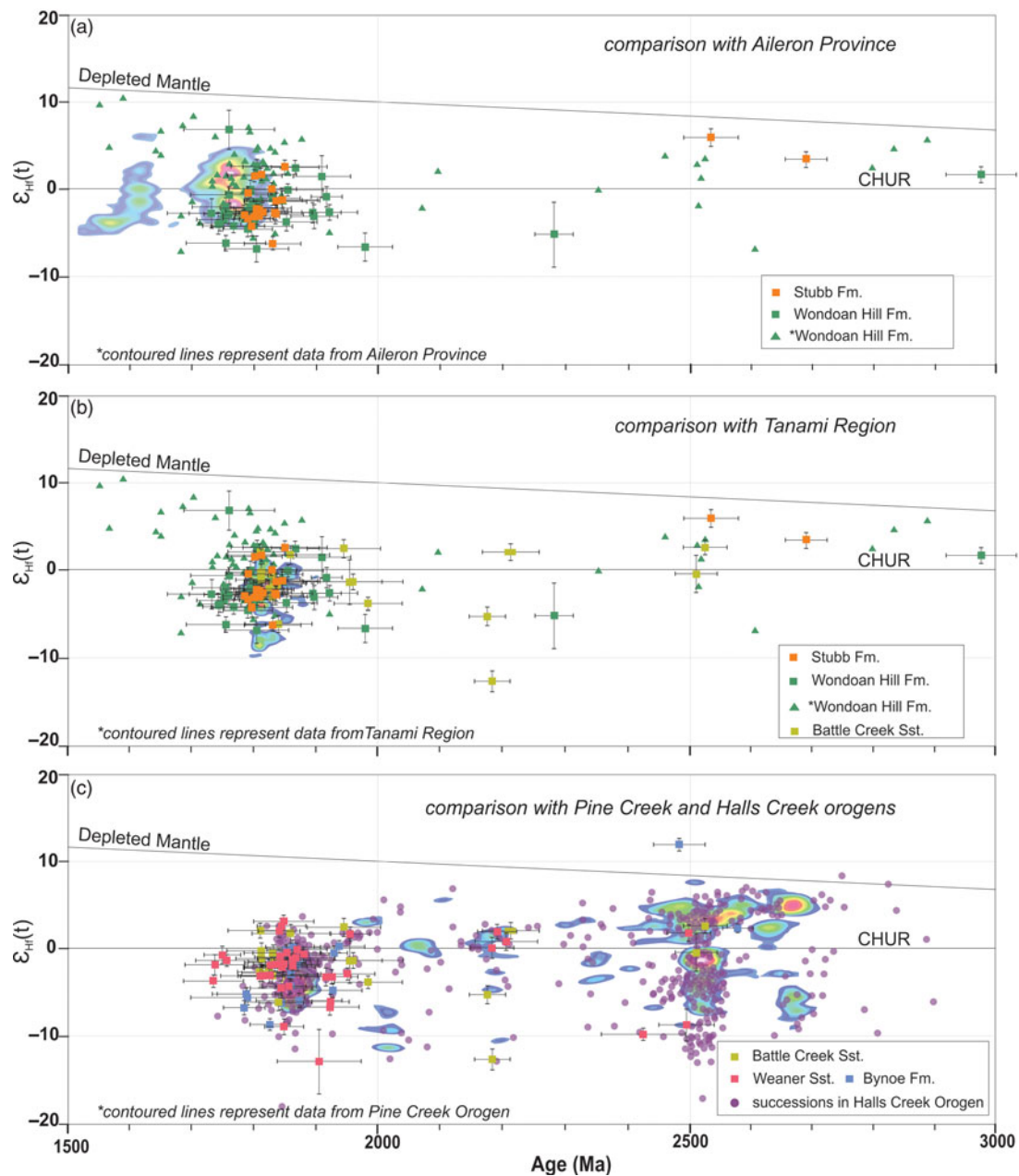
Fig. 7. Epsilon hafnium values against [207]Pb/[206]Pb ages plot of the measured samples from the Bullita Group and the Tijunna Group. Zircon $\epsilon_{Hf}(t)$ heat maps reflect the point density distribution of published magmatic zircon data from possible source regions, including (a) Aileron Province (Hollis *et al.* 2010; Beyer *et al.* 2013, 2015), (b) Tanami Region (Iaccheri, 2019) and (c) Pine Creek Orogen (Beyer *et al.* 2013). Published detrital zircon data from source regions are from Halls Creek Orogen (Hollis *et al.* 2014; Iaccheri & Kemp, 2018). CHUR: chondrite reservoir. *data from Munson *et al.* (2018).

overlap with data from all three possible source areas. The lack of comparison with the other Battle Creek sample makes the identification of potential source terrane(s) ambiguous.

4.b.2. Tijunna group

Detrital zircon data from the Tijunna Group were derived from three core samples (D57, MS-05 and MS-03; Table 1), one published drill core sample (1957137) of the Stubb Formation from Carson (2013) and one published outcrop sample (VR14TJM0003) of the Wondoan Hill Formation from Munson *et al.* (2018).

Detrital zircon age spectra of the three Wondoan Hill Formation samples all have major peaks at *c.* 1800 Ma (Fig. 4).

The prominent *c.* 1830 Ma ages seen in the Bullita Group are not so apparent in the Wondoan Hill Formation spectra (Fig. 4). This leads us to suggest that the Halls Creek and Pine Creek orogens were no longer the dominant source areas for the basin at the time of deposition of the Wondoan Hill Formation. Instead, the younger *c.* 1800 Ma zircons were mostly likely to be sourced from the Tanami Region, to the south of the basin, where *c.* 1810 Ma to 1790 Ma magmatic rocks are exposed (Fig. 4). This is supported by Hf isotope data, which have overlapping $\epsilon_{Hf}(t)$ values for *c.* 1800 Ma zircons for the Wondoan Hill Formation and the Tanami Region (Fig. 7b). The transition from the Bullita Group to the Wondoan Hill Formation is therefore interpreted to reflect
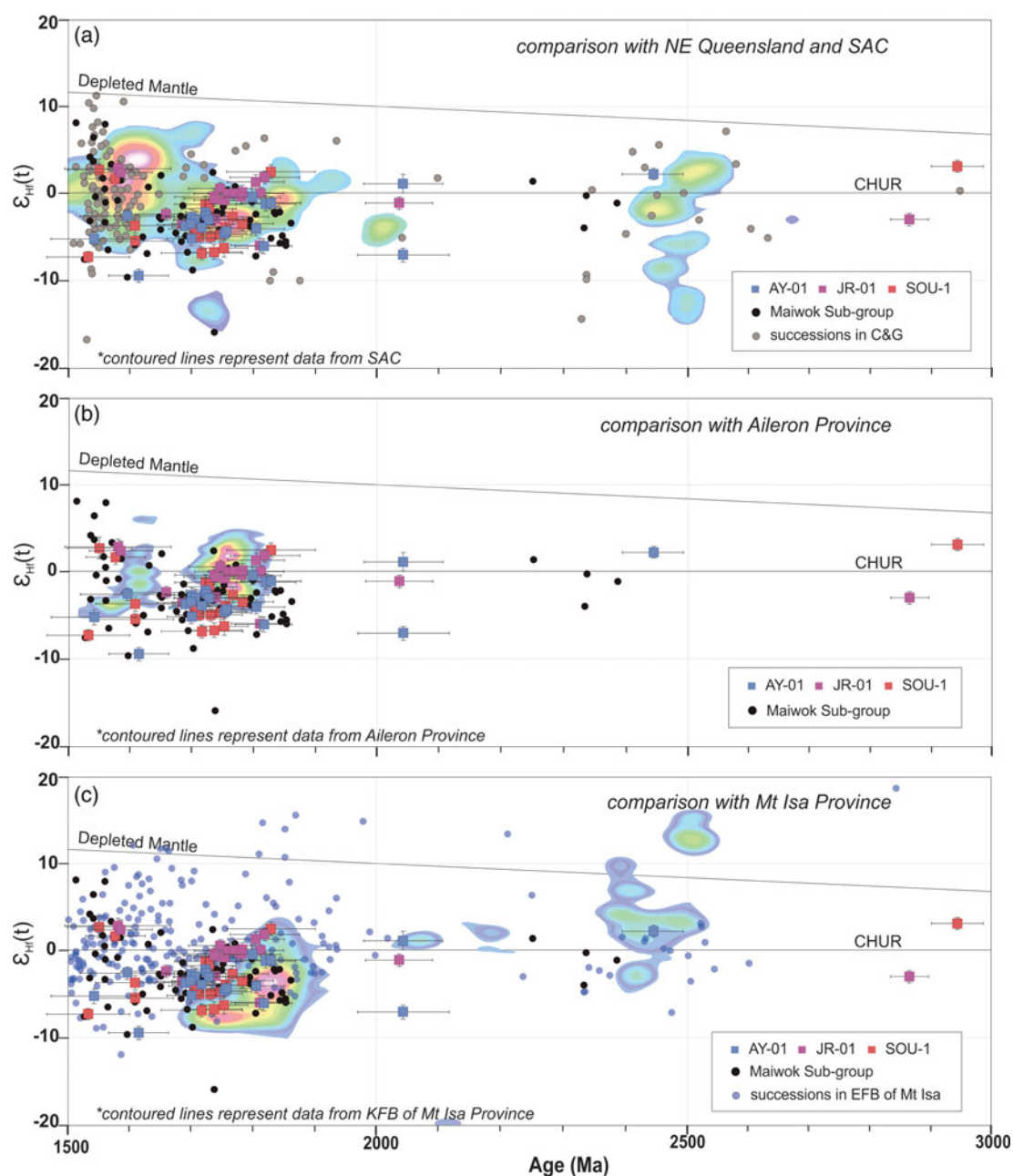
Fig. 8. Epsilon hafnium values against $^{207}Pb/^{206}Pb$ ages plot of the measured samples from the South Nicholson Group. Zircon $\epsilon_{Hf}(t)$ heat maps reflect the point density distribution of published magmatic zircon data from possible source regions, including (a) South Australian Craton (SAC; Nebel *et al.* 2007; Reid *et al.* 2008, 2014, 2017, 2020; Howard *et al.* 2009, 2011; Kromkhun *et al.* 2013; Reid & Payne, 2017), (b) Aileron Province (Hollis *et al.* 2010; Beyer *et al.* 2013, 2015), (c) the Kathleen Fold Belt (KFB) of Mount Isa Province (Bierlein *et al.* 2008). Published detrital zircon data from source regions are from the Eastern Fold Belt (EFB) of Mount Isa Province (Griffin *et al.* 2006), the Coen-Georgetown provinces (C&G; Murgulov *et al.* 2007). CHUR: chondrite reservoir. *data from Munson *et al.* (2018). Maiwok Subgroup data are from Yang *et al.* (2019).

a shift of basin provenance, from dominant northwesterly and northerly sources (e.g. Halls Creek and Pine Creek orogens) to southerly sources (e.g. Tanami Region and Aileron Province).

The two Stubb Formation samples show different zircon age spectra with differing age maxima (Fig. 4). Sample 1957131 is characterized by a major peak at *c.* 1780 Ma and two minor peaks at *c.* 1615 Ma and *c.* 1870 Ma, whereas sample MS-03 is dominated by zircon grains dated between *c.* 1830 and 1800 Ma. Potential original sources for sample 1957131 are the Aileron Province where *c.* 1790 to 1770 Ma magmatic rocks are plentiful (Fig. 4). However,

sample MS-03 has a zircon age spectrum that may reflect a mix of the Halls Creek / Pine Creek orogens as well as the Tanami Region (Fig. 4). These data suggest significant lateral or stratigraphic variation within this formation.

4.c. South Nicholson Group of the South Nicholson Basin

Detrital zircon data from the three undifferentiated South Nicholson Group samples (AY-01, SOU-01 and JR-01) were compared with the published data from Kositcin & Carson (2019) and Anderson *et al.* (2019).

Table 2. Summary of results

Basin	Borehole	Sample	Formation/Group	Analysed grains (>90 % concordant/total)	Age peaks ($\varepsilon_{Hf}(t)$ values)
McArthur Basin	Broughton-1	Bro-07	Arnold Sst. / Collara Sub-gp.	88/142	*c.* 1745 Ma (−4.6 to +4.4); *c.* 1810 Ma (−5.6 to −0.4); *c.* 1895 Ma (−2.6 to +0.1)
		Bro-06	Crawford Fm. / Collara Sub-gp.	53/107	*c.* 1780 Ma (−2.9 to −0.4)
Birrindudu Basin	99VRNTGSDD2	D57	Wondoan Hill Fm. / Tijunna Gp	46/109	*c.* 1795 Ma (−4.1 to +2.6); *c.* 1840 Ma (−3.8 to +2.5)
		D24	Weaner Sst. / Bullita Gp	23/109	*c.* 1730 Ma (−3.7 to −0.7); *c.* 1830 Ma (−9.0 to +3.2); *c.* 1940 Ma (−6.1 to +1.7)
		D02	Bynoe Fm. / Bullita Gp	48/98	*c.* 1780 Ma (−6.8 to −5.2); *c.* 1835 Ma (−8.7 to +0.2); *c.* 1920 Ma (−4.8 to +0.2)
	MSFD001	MS-03	Stubb Fm. / Tijunna Gp	49/133	*c.* 1810 Ma (−4.3 to +1.7)
		MS-05	Wondoan Hill Fm. / Tijunna Gp	53/118	*c.* 1795 Ma (−6.8 to −0.2)
		MS-06	Battle Creek Sst. / Bullita Gp	41/124	*c.* 1810 Ma (−6.1 to +2.1)
		MS-09	Weaner Sst. / Bullita Gp	44/102	*c.* 1830 Ma (−4.4 to +2.6); *c.* 1910 Ma (−13.0 to −3.2)
South Nicholson Basin	AY06DD01	AY-01	Undifferentiated / South Nicholson Gp	73/122	*c.* 1715 Ma (−5.3 to −2.2); *c.* 1810 Ma (−6.1 to −0.5)
	NTGS00-1	SOU-01	Undifferentiated / South Nicholson Gp	53/86	*c.* 1600 Ma (−3.0 to +0.5); *c.* 1760 Ma (−6.9 to −1.3)
	NTGS01-1	JR-01	Undifferentiated / South Nicholson Gp	46/121	*c.* 1770 Ma (−6.3 to −2.7)

Gp: Group; Fm: Formation; Sst: Sandstone.

The detrital zircon age spectra of the three undifferentiated South Nicholson Group samples, along with the published data from the Crow Formation and the Constance Sandstone, are all dominated by *c.* 1790 to 1700 Ma zircon grains (Fig. 5). These age spectra are comparable to the ages of rocks found in the Mount Isa and Aileron provinces (Fig. 5). The slightly evolved hafnium isotope signatures ($\varepsilon_{Hf}(t)$: −7 to +3) of those *c.* 1790–1700 Ma zircon grains are also consistent with these areas being sources (Fig. 8). In addition, the three undifferentiated samples, more or less, all preserve zircon grains with ages between *c.* 1600 and 1550 Ma. These zircon grains, together, yield a spread of $\varepsilon_{Hf}(t)$ values that form a vertical array (ranging from −9.5 to +2.8), which is comparable to zircon hafnium isotopic ranges from the eastern Mount Isa Province, Georgetown Province and South Australian Craton (SAC; Fig. 8a). We suggest that the samples from the South Nicholson Group mainly received detritus from Mount Isa Province, with possible contributions from the Aileron Province. Some detritus might also have been derived from the Coen–Georgetown regions in the northeastern NAC and SAC, which are interpreted to have been adjacent to one another during the Mesoproterozoic from palinspastic reconstructions (e.g. Li & Evans, 2011; Nordsvan *et al.* 2018; Fig. 9).

5. Discussion

5.a. Tectonic geography of the Roper Group

Detrital zircon U–Pb and hafnium isotope data suggest that the three sampled formations of the Collara Subgroup (Crawford Formation, Arnold Sandstone and Hodgson Sandstone; Figs. 3,

6) were predominantly sourced from the Mount Isa Province to the southeast and Aileron Province to the south. Their consistent zircon age spectra indicate little variation of provenance through time. However, the upward transition into the Maiwok Subgroup is marked by a distinct provenance variation, shown by an increase in *c.* 1.6–1.5 Ga zircon grains (Fig. 3). Yang *et al.* (2018, 2019) interpreted these zircons to be sourced from the Eastern Fold Belt (EFB) of Mount Isa, or even more distal sources in the Coen–Georgetown region and the South Australian Craton (SAC). In the MDS plot (Fig. 10), the Collara Subgroup formations plot close to the Mount Isa (WFB&KFB) and Aileron provinces, whereas the Maiwok Subgroup samples, with more *c.* 1.6 Ga ages, are closer to the EFB of Mount Isa, Coen–Georgetown region and SAC. Cawood & Korsch (2008) and Payne *et al.* (2009) suggest that the North and South Australia cratons, as well as the bulk of the Mawson continent, were joined at least until the early Mesoproterozoic, forming what is called the Diamantina Craton. Proterozoic plate reconstructions (Li & Evans, 2011; Nordsvan *et al.* 2018) suggest that the Mount Isa, Coen–Georgetown and SAC regions lined the eastern margin of this Diamantina Craton in Mesoproterozoic times (Fig. 9). A few *c.* 1.6–1.5 Ga zircon grains occur in the Collara Subgroup, but a relative increase in the number of these grains within the Maiwok Subgroup samples suggests that easterly source terranes were more tectonically active at this time and were being exhumed and eroded. This exhumation is recorded by a series of low-temperature mineral cooling ages in the proposed source areas that are coeval with deposition of the Maiwok Subgroup. They include white mica and biotite ^{40}Ar–^{39}Ar ages of *c.* 1.46–1.38 Ga from the Eastern Fold Belt (Spikings *et al.* 2001), apatite U–Pb ages of *c.* 1.47–1.40 Ga from the northern SAC
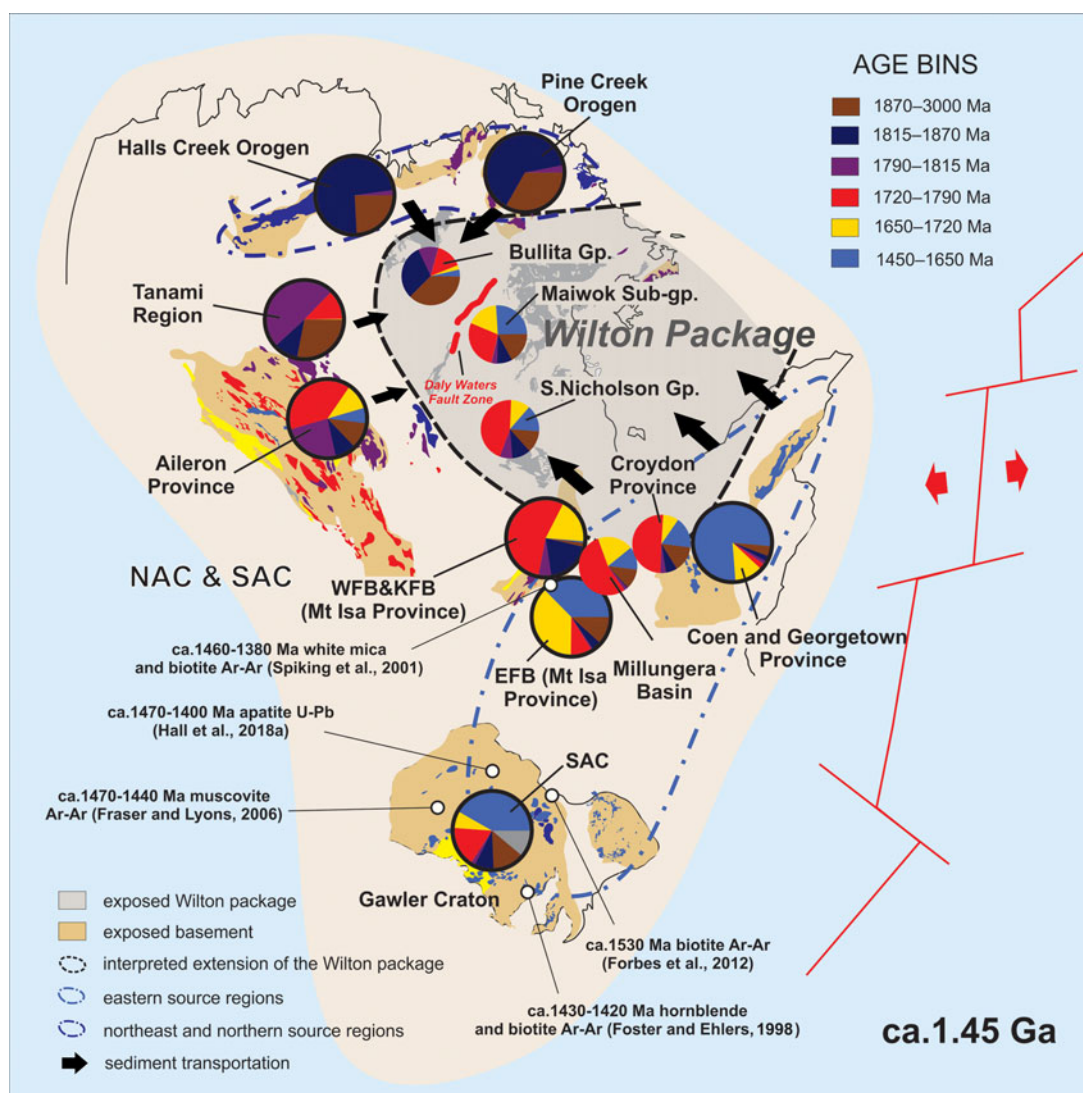
Fig. 9. Reconstruction of the Mesoproterozoic North Australian Craton (NAC) and South Australian Craton (SAC) at *c.* 1.45 Ga, modified after Yang et al (2018, 2019). The proposed exhumation of eastern source regions during the separation between the NAC–SAC and Laurentia is shown. Compiled zircon age distributions from sedimentary units and potential sources plotted as pie diagrams, following the method proposed by Sharman *et al.* (2018). Large pie charts with black outlines are possible source regions; smaller pie charts with no outline are sediment age distributions in the Wilton package and coeval sedimentary sequences. Colours of pie charts and igneous units refer to age bins in the legend (see Fig. 10).

(Hall *et al.* 2018*a*), apatite U–Pb ages of *c.* 1.66–1.54 Ga from the northeast SAC (Hall *et al.* 2018*b*), biotite ^{40}Ar–^{39}Ar ages of *c.* 1.53 Ga from the NE Gawler Craton (Forbes *et al.* 2012), and hornblende and biotite ^{40}Ar–^{39}Ar ages of *c.* 1.43–1.42 Ga from the SE Gawler Craton (Foster & Ehlers, 1998; Fig. 9). Yang *et al.* (2018, 2019) suggested that this exhumation may have been the result of rifting between the NAC–SAC terranes and Laurentia at *c.* 1.45 Ga. Relative uplift of the rift shoulders resulted in the eastern source areas becoming topographic highs; this modified the ancient geography and basin drainage system, so as to deliver considerably more detritus from these areas (highlighted by the *c.* 1.6–1.5 Ga zircon grains) to the Maiwok Subgroup.

5.b. Tectonic geography of Bullita and Tijunna groups

Provenance analysis suggests that the Bullita Group was mainly sourced from northerly and northwesterly sources (e.g. Pine

Creek and Halls Creek orogens), whereas the Tijunna Group received detritus from source regions to the south of the basin (e.g. Tanami Region and Aileron Province; Fig. 1c). This provenance evolution is well reflected in a graph probability distribution plot (Fig. 11) following Eglington (2018), which shows that the late Palaeoproterozoic age maxima for the younger formations gradually changes from *c.* 1.83 Ga to *c.* 1.80 Ga. This switch in provenance is demonstrated in an MDS plot (Fig. 10), in which the Bullita Group samples plot close to the Halls Creek and Pine Creek orogens, whereas the younger Tijunna Group samples, with higher proportions of *c.* 1.80 Ga zircon analyses, plot closer to the Tanami Region. This stratigraphic change in provenance is particularly evident when samples from individual drill cores are examined, which removes any possible spatial variation in source. Samples D02, D24, 1957143, D57 and 1957137 all came from core 99VRNTGSDD2, whereas samples MS-09, MS-06, MS-05 and MS-03 all came from core MSFD001 (Table 1). These two
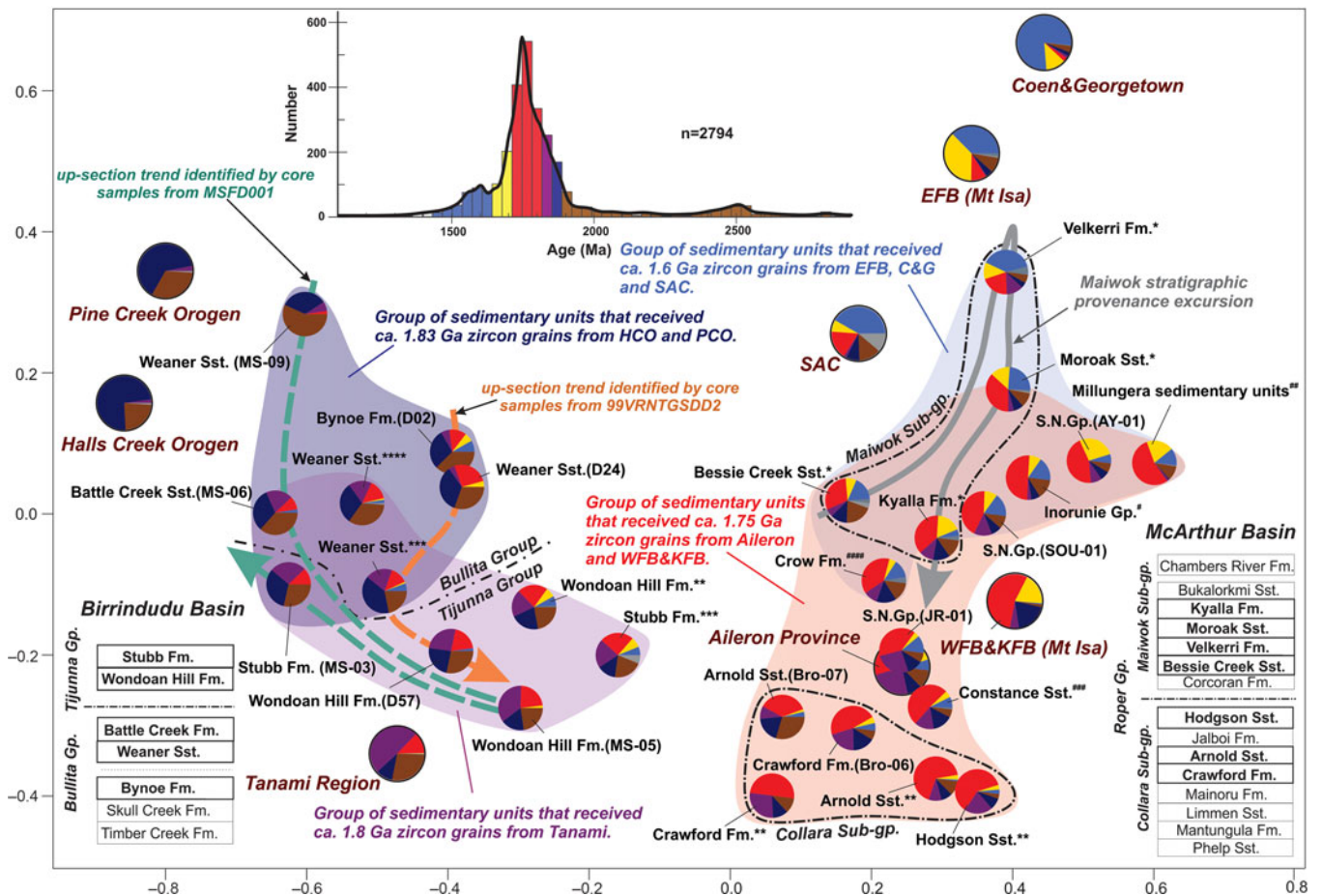
Fig. 10. Joint non-parametric multidimensional scaling (MDS) plot (after Vermeesch, 2013) showing the relationships amongst analysed formations. Compiled zircon age distributions from sedimentary units and potential sources plotted as pie diagrams, following the method proposed by Sharman *et al.* (2018). The larger pie charts with black outlines are the potential source areas. Detrital zircon ^{207}Pb/^{206}Pb age data included in this study are from *Yang *et al.* (2018, 2019), **Munson *et al.* (2018), ***Carson (2013), ****Kositcin & Carson (2017), #Nordsvan *et al.* (2018), ##Neumann & Kositcin (2011), ###Anderson *et al.* (2019) and ####Kositcin & Carson (2019). SAC: South Australian Craton; WFB: Western Fold Belt (Mount Isa Province); KFB: Kathleen Fold Belt (Mount Isa Province); EFB: Eastern Fold Belt (Mount Isa Province); Fm: Formation; Sst: Sandstone; Gp: Group. Pie chart colours refer to age bins defined on the KDE plot of all near-concordant U–Pb age detrital age data (top).

cores exhibit similar up-section trends from older samples derived from the Halls Creek and Pine Creek orogens to younger samples with closer affinities to the Tanami Region (Fig. 10). Further, in the MDS plot (Fig. 10), the Wondoan Hill Formation samples are relatively more clustered, compared to the underlying Bullita samples. This might highlight a consistent detrital input into the Wondoan Hill system and suggests that the deposition of this formation was laterally homogeneous and continuous. We interpret this homogeneity to represent uplift and erosion of the Tanami Region, swamping the basin with southerly-sourced sediments. Detrital zircon age spectra from the overlying Stubb Formation show a return to local heterogeneity, which may reflect the waning influence of southern sources, or perhaps the recycling of older sedimentary rocks (e.g. Bullita Group) during source area uplift.

A similar stratigraphic southward shift in provenance is evident in the Maiwok Subgroup (Roper Group) samples from the Beetaloo Sub-basin. Yang *et al.* (2018, 2019) used detrital zircon U–Pb and Hf data to suggest that formations in the lower parts of the subgroup (e.g. Bessie Creek Sandstone, Velkerri Formation and Moroak Sandstone) were sourced from

southeasterly and easterly sources (e.g. Mount Isa Region, Coen–Georgetown region and SAC), whereas the Kyalla Formation at the top of the Maiwok Subgroup received detritus from the Aileron Province to the south of the basin (Figs 9, 12). Yang *et al.* (2018, 2019) suggested that this shift to southern sources may be related to a closure of the ocean that separated the combined NAC–SAC from the West Australian Craton (WAC) (named the Mirning Ocean; Fig. 12; Kirkland *et al.* 2015). We hypothesize that during its closure, the present-day southern margin of the NAC was uplifted and eroded. These regions became the southern sources (e.g. Aileron Province and Tanami Region), which fed sediment into the greater McArthur Basin through a north-flowing drainage system (Fig. 12). The closure of this ocean is marked by *c.* 1.40 to 1.20 Ga subduction-related magmatism (Kirkland *et al.* 2015; Spaggiari *et al.* 2015; Morrissey *et al.* 2017), orogenesis (Johnson *et al.* 2013; Howard *et al.* 2015) and metamorphism (Anderson, 2015; Morrissey *et al.* 2017) that occurred along the boundary between the WAC and the NAC–SAC (Fig. 12).

The *c.* 1.40 to 1.35 Ga ocean closure/subduction related arc-volcanism (Kirkland *et al.* 2015) is temporally consistent with the
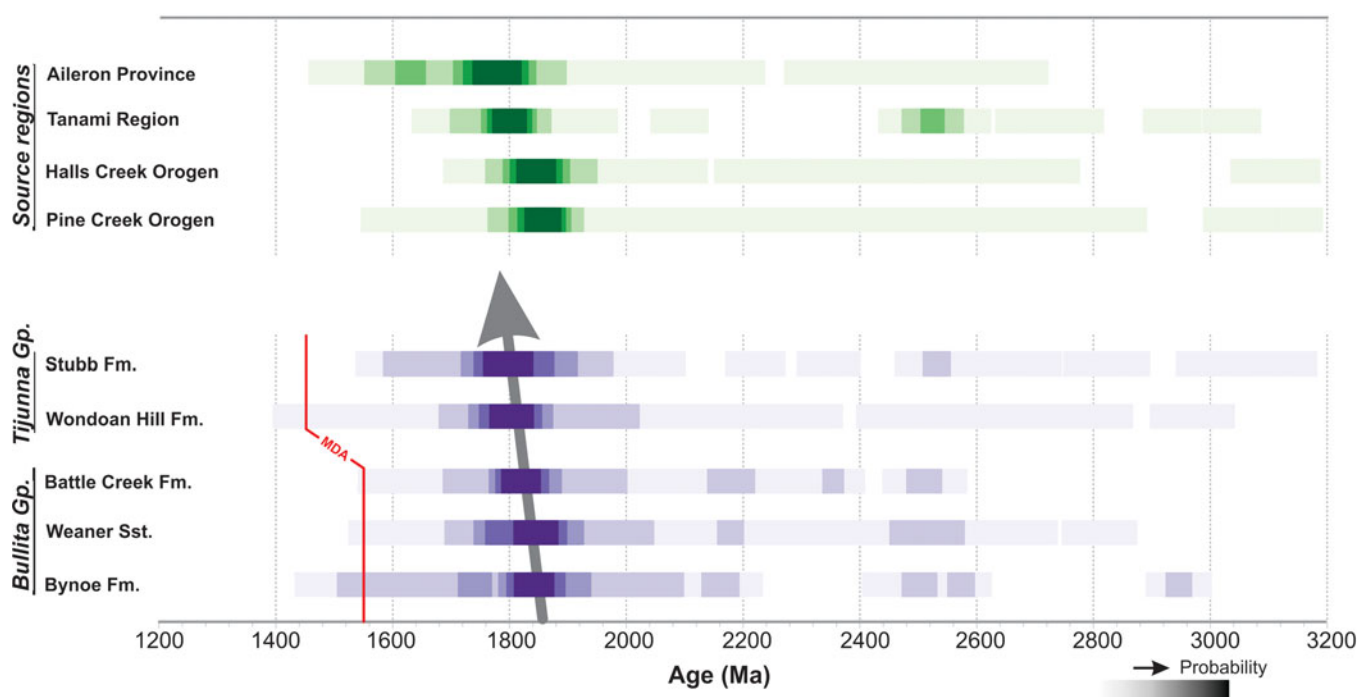
Fig. 11. Graph probability distribution plot comparing the composed detrital zircon age spectra of formations from the Bullita and Tijunna groups. The plot was generated using the FitPDF program (Eglington, 2018). Probabilities are illustrated by the colour density. MDA: maximum deposition age; Gp: Group; Fm: Formation. Red line represents assigned maximum deposition age for each formation. Grey line represents the stratigraphic shifting of the dominant age peaks.

juvenile neodymium isotopic compositions in the middle Velkerri Formation (Cox *et al.* 2016, 2019). This is argued to represent the erosional products of the arc volcanic rocks, while the basin provenance shifted from predominately eastern sources to southern sources. The delivery of the arc volcanic detritus is suggested to have resulted in high nutrient supply to the basin, enhancing the biological primary productivity, and subsequent high organic carbon burial within the middle Velkerri Formation (Cox *et al.* 2016, 2019).

5.c. Basin correlations within the Wilton package

The youngest detrital zircon grains from the undifferentiated South Nicholson Group samples have ^{207}Pb/^{206}Pb dates of 1519 ± 51 Ma (sample JR-01), 1550 ± 51 Ma (sample SOU-01) and 1542 ± 69 Ma (sample AY-01). This constrains the depositional ages of the sampled units to be later than *c.* 1550 Ma, which is consistent with interpreted maximum depositional ages determined for the Playford Sandstone and Crow Formation (1600 ± 20 Ma and 1483 ± 12 Ma respectively; Kositcin & Carson, 2019), and suggests that the undifferentiated units might represent subsurface extensions of these formations. These age constraints for the South Nicholson Group are also comparable to those for the Collara Subgroup, which was deposited after *c.* 1.5 Ga (Jackson *et al.* 1999; Munson, 2016).

In the MDS plot (Fig. 10), the Collara Subgroup, Maiwok Subgroup and the South Nicholson Group samples form a tight group that is distinct from the Birrindudu Basin formations. They are more similar to the Mount Isa Province and the Aileron Province. In the $\epsilon_{Hf}(t)$ vs age plots (Figs 6, 8), the South Nicholson Group and Roper Group data (including the Collara and Maiwok subgroups) overlap with each other. These similarities in age and isotope geochemistry strongly support a correlation

between the Roper and South Nicholson groups and suggest that there was a sedimentary pathway connection between the McArthur–Beetaloo basins and the South Nicholson Basin at the time of deposition of these groups.

The Inorunie Group of the Croydon Province (Fig. 1), to the east of the Mount Isa Province, is a *c.* 1500 Ma siliciclastic succession that is remarkably similar to the Wilton package. Sandstones from this group are interpreted to have been sourced from the Mount Isa Province (Figs 1, 10; Budd *et al.* 2002; Withnall & Hutton, 2013; Nordsvan *et al.* 2018) and were deposited in a basin that may be coeval to, and in a similar tectonic setting to, the Roper and South Nicholson basins (Fig. 10). The poorly known Millungera Basin (Fig. 1) may also be an extension of this depositional system, on the basis of detrital zircon chronology (Fig 10). In the probability distribution plot (Fig. 13), the sedimentary rocks from the Inorunie Group of the Croydon Province and the Millungera Basin exhibit significant consistency with the samples from the Roper and South Nicholson groups.

The provenance of the Roper and South Nicholson groups (Beetaloo Sub-basin and South Nicholson Basin) are quite different to those of the coeval Bullita and Tijunna groups (Birrindudu Basin). The Birrindudu Basin rocks were sourced from the Halls Creek – Pine Creek orogens and Tanami–Aileron regions, whereas the eastern sedimentary formations were sourced from the Mount Isa, Coen–Georgetown, SAC and Aileron regions (to the east and southeast). The MDS plot clearly shows this dissimilarity (Fig. 10). We suggest that the ancestral Daly Waters Fault Zone was a palaeo-bathymetric high at the time and divided the two parts of the greater McArthur Basin (Figs 1 and 2). This interpretation is supported by seismic data that shows considerable thickness and geometric differences between the Wilton package west and east of the Daly Waters Fault Zone (Williams, 2019; Figs 1, 2). This bathymetric high restricted sediment mixing across it, isolating the
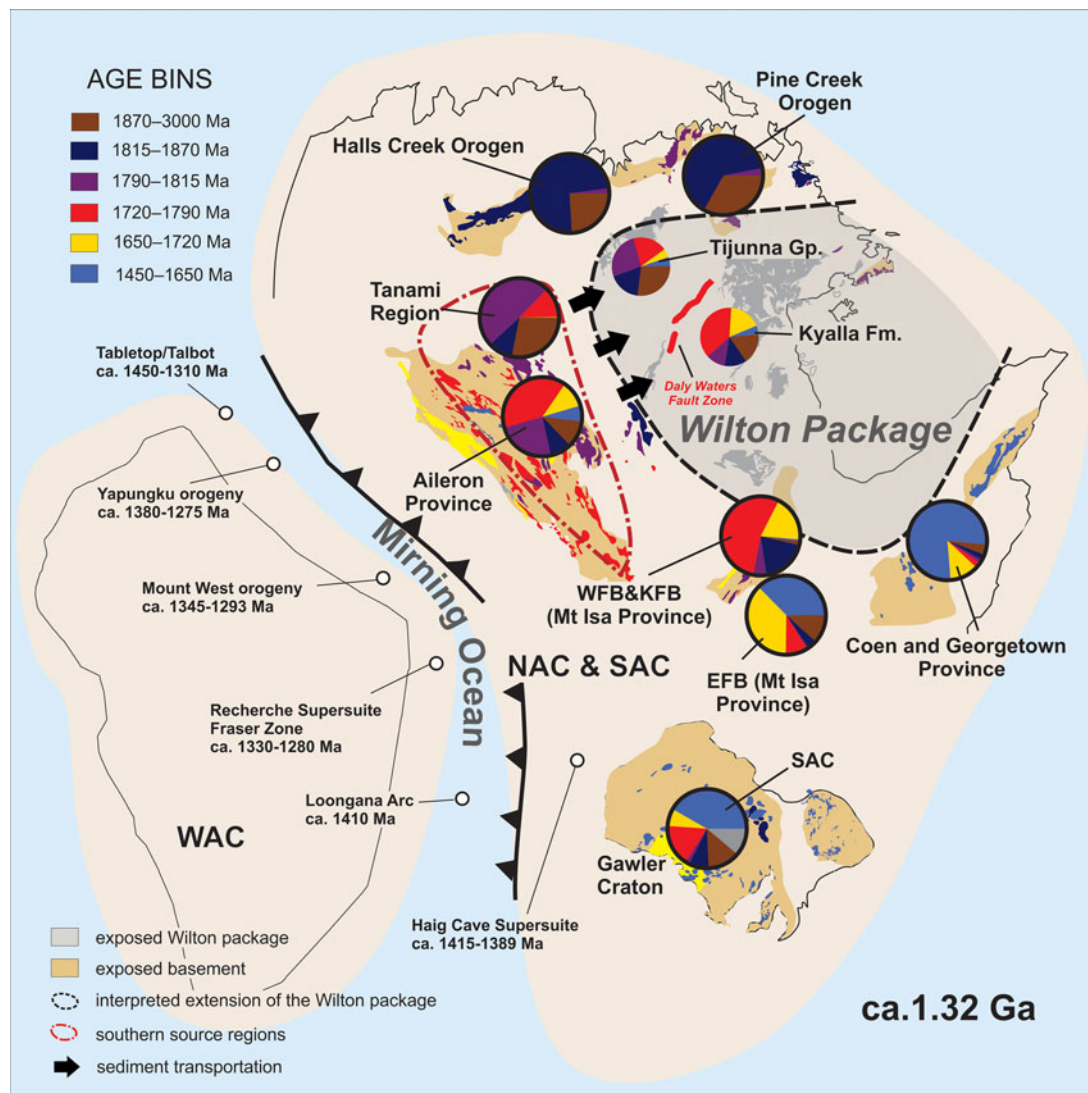
Fig. 12. Reconstruction of Australia at *c.* 1.32 Ga. The reconstruction shows the uplift and exposure of southern sources (e.g. the Aileron Province and Tanami Region) during the amalgamation of the West Australian Craton (WAC) with the North and South Australian cratons (NAC–SAC). This allowed them to become sources for the upper Maiwok Subgroup and the Tijunna Group (modified after Yang *et al.* 2019). Compiled zircon age distributions from sedimentary units and potential sources plotted as pie diagrams, following the method proposed by Sharman *et al.* (2018). Large pie charts with black outlines are possible source regions; smaller pie charts with no outline are sediment age distributions in the Wilton package and coeval sedimentary sequences. Colours of pie charts and igneous units refer to age bins in the legend (see Fig. 10).

Birrindudu Basin in the west from the eastern Beetaloo Sub-basin and South Nicholson Basin.

6. Conclusions

Coupled detrital zircon U–Pb age and Lu–Hf isotope data presented in this study of the North Australian Craton from *c.* 1.55 to 1.31 Ga provide new constraints on inter-basinal and intra-basinal correlations and sedimentary provenance. This study illustrates the dynamic interactions between sedimentary and tectonic processes, and enhances palaeogeographic reconstructions.

We suggest that the Collara Subgroup (lower Roper Group) was sourced from the Mount Isa Province and Aileron Province. Rifting between the NAC–SAC and Laurentia, after the deposition of the Collara Subgroup, caused uplift in the east (e.g. the Eastern Fold Belt (EFB) of the Mount Isa Province, and the Coen–Georgetown region and palinspastically adjacent South

Australian Craton), which shed detritus west into the lower Maiwok Subgroup depositional system.

Provenance consistency between the South Nicholson Group and the Roper Group (of the South Nicholson Basin and Beetaloo Sub-basin, respectively) indicates that they were sourced from similar areas and are likely part of the same depositional system (linked basins). We note that the *c.* 1.5 Ga Inorunie Group of the Croydon Province, and the Millungera Basin succession are possible correlatives of the Wilton package and have similar-aged detritus, suggesting they may form an analogous coeval depositional system in a comparable tectonic setting, but to the east of the then uplifted Mount Isa Province.

The Bullita and Tijunna groups of the Birrindudu Basin have a different provenance than the Roper and South Nicholson groups. Provenance analysis shows that the Bullita Group was sourced from northeastern and northern sources (Halls Creek Orogen and Pine Creek Orogen), whereas the Tijunna Group received
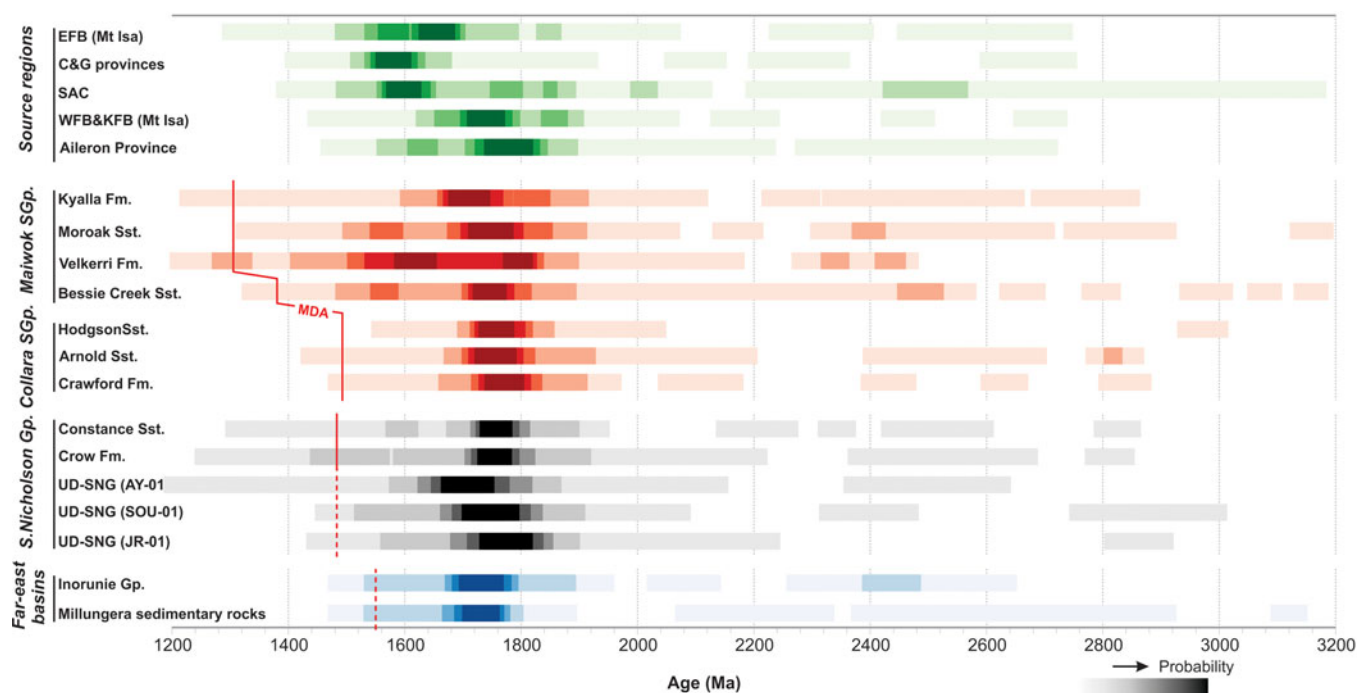
Fig. 13. Graph probability distribution plot of the composite detrital zircon age spectra of formations from the Maiwok Subgroup, Collara Subgroup, South Nicholson Group, Inorunie Group and sedimentary rocks from the Millungera Basin (Fig. 1), illustrating the provenance similarity between these basins. The plot was generated using the FitPDF program (Eglington, 2018). Probabilities are illustrated by the colour density. MDA: maximum deposition age; Gp: group; Fm: formation. Red lines represent assigned maximum deposition age for each formation. Red dashed lines represent possible maximum deposition age constraint.

more detritus from southern sources (Tanami Region and Aileron Province). Provenance differences between the Birrindudu Basin and eastern Beetaloo Sub-basin support interpretations that the intervening meridional Daly Waters Fault Zone was a significant positive bathymetric feature at the time (Williams, 2019).

Despite this largely independent early depositional history, stratigraphically higher formations within both the Beetaloo Sub-basin and Birrindudu Basin record southward shifts in sediment source areas. We suggest that both areas were buried by sediment eroded from the south during the amalgamation of the NAC–SAC and the WAC at *c.* 1.35 to 1.28 Ga. This resulted in uplift of the southern margin of the NAC and modification of the basin geography and drainage system. It is likely that the subduction and closure of the Mirning Ocean is responsible for uplift and erosion along the southern part of the NAC. This engendered northern-flowing river systems that transported sediment eroded from this region into both the Birrundudu Basin and the Beetaloo Sub-basin.

Conflict of interest. None.

Supplementary material. To view supplementary material for this article, please visit https://doi.org/10.1017/S0016756820001223

References

Abbott ST and Sweet IP (2000) Tectonic control on third-order sequences in a siliciclastic ramp-style basin: an example from the Roper Superbasin (Mesoproterozoic), northern Australia. *Australian Journal of Earth Sciences* **47**, 637–57.

Abbott ST, Sweet IP, Plumb KA, Young DN, Cutovinos A, Ferenczi PA and Pietsch BA (2001) Roper Region: Urapunga and Roper River Special, Northern Territory (Second Edition). 1:250 000 geological map series explanatory notes, SD 53-10, 11. *Northern Territory Geological Survey and Geoscience Australia (National Geoscience Mapping Accord).*

Ahmad M and Munson TJ (2013) Geology and Mineral Resources of the Northern Territory. *Northern Territory Geological Survey* **5**.

Allen JF, Thake B and Martin WF (2019) Nitrogenase inhibition limited oxygenation of Earth's Proterozoic atmosphere. *Trends in Plant Science* **24**, 1022–31.

Anderson J (2015) *Metamorphic and isotopic characterisation of Proterozoic belts at the margins of the North and West Australian Cratons.* Adelaide, South Australia: University of Adelaide.

Anderson JR, Lewis CJ, Jarrett AJM, Carr L, Henson P, Carson C, Southby C and Munson T (2019) New SHRIMP U-Pb zircon ages from the South Nicholson Basin, Mout Isa Orogen, and Georgina Basin, Northern Territory and Queensland. *Geoscience Australia, Record* **10**.

Bagas L, Bierlein FP, Anderson JAC and Maas R (2010) Collision-related granitic magmatism in the Granites-Tanami Orogen, Western Australia. *Precambrian Research* **177**, 212–26.

Beyer EE, Allen CM, Armstrong R and Woodhead JD (2015) Summary of results. NTGS laser ablation ICPMS and SHRIMP U-Pb, Hf and O geochronology project: Pine Creek Orogen, Arunta Region, Georgina Basin and McArthur Basin, July 2008–May 2011. *Northern Territory Geological Survey, Record* 2012-007.

Beyer EE, Donnellan N, Meffre S and Thompson JM (2016) Summary of results. NTGS laser ablation ICP-MS in situ zircon and baddeleyite

geochronology project: Mount Peake Gabbro, Arunta Region. *Northern Territory Geological Survey, Record* 2016-002.

Beyer EE, Hollis JA, Whelan JA, Glass LM, Donnellan N, Yaxley G, Armstrong R, Allen C and Scherstén A (2013) Summary of results. NTGS laser ablation ICPMS and SHRIMP U-Pb, Hf and O geochronology project: Pine Creek Orogen, Arunta Region, Georgina Basin and McArthur Basin, July 2008–May 2011. *Northern Territory Geological Survey, Record* 2012-007.

Bierlein FP, Black LP, Hergt J and Mark G (2008) Evolution of Pre-1.8 Ga basement rocks in the western Mt Isa Inlier, northeastern Australia – insights from SHRIMP U-Pb dating and in-situ Lu-Hf analysis of zircons. *Precambrian Research* 163, 159–73.

Blewett RS, Black LP, Sun SS, Knutson J, Hutton LJ and Bain JHC (1998) U-Pb zircon and Sm-Nd geochronology of the Mesoproterozoic of North Queensland: implications for a Rodinian connection with the Belt supergroup of North America. *Precambrian Research* 89, 101–27.

Bodorkos S, Beyer EE, Edgoose CJ, Whelan JA, Webb G, Vandenberg LC and Hallett L (2013) Summary of results. Joint NTGS–GA geochronology project: central and eastern Arunta Region, January 2008–June 2011. *Northern Territory Geological Survey, Record* 2013-003.

Bodorkos S, Crowley JL, Claoué-Long J, Anderson JR and Magee CWJ (2020) Precise U-Pb baddeleyite dating of the Derim Derim Dolerite, McArthur Basin, Northern Territory: old and new SHRIMP and ID-TIMS constraints. *Australian Journal of Earth Sciences*. doi: 10.1080/08120099.2020.1749929

Bouvier A, Vervoort JD and Patchett PJ (2008) The Lu-Hf and Sm-Nd isotopic composition of CHUR: constraints from unequilibrated chondrites and implications for the bulk composition of terrestrial planets. *Earth and Planetary Science Letters* 273, 48–57.

Budd AR, Wyborn LAI and Bastrakova IV 2002. The metallogenic potential of Australian Proterozoic granites [Summary Volume]. *Geoscience Australia. Record* 2001/12, 1–152.

Butterfield NJ (2015) Early evolution of the Eukaryota. *Palaeontology* 58, 5–17.

Carson CJ 2013. The Victoria and Birrindudu Basins, Victoria River region, Northern Territory, Australia: a SHRIMP U-Pb detrital zircon and Sm-Nd study. *Australian Journal of Earth Sciences* 60, 175–96.

Carson CJ, Claoué-Long J, Stern R, Close DF, Scrimgeour IR and Glass LM 2009. Summary of results. Joint NTGS-GA geochronology project: central and eastern Arunta Region and Pine Creek Orogen, July 2006–May 2007. *Northern Territory Geological Survey, Record* 2009-001.

Cawood PA and Korsch RJ 2008. Assembling Australia: Proterozoic building of a continent. *Precambrian Research* 166, 1–35.

Close DF 2014. The McArthur Basin: NTGS' approach to a frontier petroleum basin with known base metal prospectivity. In *'Annual Geoscience Exploration Seminar (AGES). Record of abstracts'. Northern Territory Geological Survey, Record* 2014-001.

Cox GM, Jarrett A, Edwards D, Crockford PW, Halverson GP, Collins AS, Poirier A and Li ZX (2016) Basin redox and primary productivity within the Mesoproterozoic Roper Seaway. *Chemical Geology* 440, 101–14.

Cox GM, Sansjofre P, Blades ML, Farkas J and Collins AS (2019) Dynamic interaction between basin redox and the biogeochemical nitrogen cycle in an unconventional Proterozoic petroleum system. *Scientific Reports* 9.

Cross AJ, Claoué-Long JC, Scrimgeour IR, Ahmad M and Kruse PD 2005a. Summary of results. Joint NTGS-GA geochronology project: Rum Jungle, basement to southern Georgina Basin and eastern Arunta Region 2001–2003. *Northern Territory Geological Survey, Record* 2005-006.

Cross AJ, Claoué-Long JC, Scrimgeour IR, Close DF and Edgoose CJ 2005b. Summary of results. Joint NTGS-GA geochronology project: southern Arunta Region. *Northern Territory Geological Survey, Record* 2004-003.

Cross AJ, Claoué-Long JC, Scrimgeour IR, Crispe A and Donnellan N 2005c. Summary of results. Joint NTGS-GA geochronology project: northern Arunta and Tanami regions, 2000–2003. *Northern Territory Geological Survey, Record* 2005-003.

Cross AJ, Purdy DJ, Bultitude RJ, Brown DD and Carr PA 2015. Summary of results. Joint GSQ–GA geochronology project: Thomson Orogen, New England Orogen, Mossman Orogen and Mount Isa region, 2011–2013. *Queensland Geological Record* 2016/03.

Eglington BM (2018) *FitPDF : a program to calculate and graph probability curves for data measurements with uncertainties.* Saskatoon, Saskatchewan: Saskatchewan Isotope Laboratory, pp. 1–17.

Fanning CM (2012) SHRIMP U–Pb zircon age determinations on detrital zircons from drill core sample ALT-051. ANU Research School of Earth Sciences, PRISE Report 12-260. Esso Australia. *Northern Territory Geological Survey, Core Sampling Report* CSR0211.

Forbes CJ, Giles D, Jourdan F, Sato K, Omori S and Bunch M (2012) Cooling and exhumation history of the northeastern Gawler Craton, South Australia. *Precambrian Research* 200–203, 209–38.

Foster DA and Ehlers K (1998) $^{40}Ar/^{39}Ar$ thermochronology of the southern Gawler Craton, Australia: implications for Mesoproterozoic and Neoproterozoic tectonics of East Gondwana and Rodinia. *Journal of Geophysical Research* 103, 10177–10193. doi: 10.1029/98JB00151

Frogtech Geoscience (2018) SEEBASE® study and GIS for greater McArthur Basin. Northern Territory Geological Survey, Digital Information Package DIP 017. https://geoscience.nt.gov.au/gemis/ntgsjspui/handle/1/87064

Griffin WL, Belousova EA, Walters SG and O'Reilly SY 2006. Archaean and Proterozoic crustal evolution in the Eastern Succession of the Mt Isa district, Australia: U-Pb And Hf-isotope studies of detrital zircons. *Australian Journal of Earth Sciences* 53, 125–49.

Hall JW, Glorie S, Reid AJ, Boone SC, Collins AS and Gleadow A (2018b) An apatite U–Pb thermal history map for the northern Gawler Craton, South Australia. *Geoscience Frontiers* 9, 1293–308.

Hall JW, Glorie S, Reid AJ, Collins AS, Jourdan F, Danisik M and Evans N (2018a) Thermal history of the northern Olympic Domain, Gawler Craton; correlations between thermochronometric data and mineralising systems. *Gondwana Research* 56, 90–104.

Hollis JA, Beyer EE, Whelan JA, Kemp AIS, Scherstén A and Greig A 2010. Summary of results. NTGS laser U–Pb and Hf geochronology project: Pine Creek Orogen, Murphy Inlier, McArthur Basin and Arunta Region, July 2007–June 2008. *Northern Territory Geological Survey, Record* 2010-001.

Hollis JA, Kemp AIS, Tyler IM, Kirkland CL, Wingate MTD, Phillips C, Sheppard S, Belousova E and Gréau Y (2014) Basin formation by orogenic collapse: zircon U–Pb and Lu–Hf isotope evidence from the Kimberley and Speewah Groups, northern Australia. In *Geological Survey of Western Australia Report*. Perth: Geological Survey of Western Australia, p. 46.

Hoskin PWO and Black LP (2000) Metamorphic zircon formation by solid-state recrystallisation of protolith igneous grains. *Journal of Metamorphic Geology* 18, 423–39.

Howard HM, Smithies RH, Kirkland CL, Kelsey DE, Aitken A, Wingate MTD, de Gromard RQ, Spaggiari CV and Maier WD (2015) The burning heart – the Proterozoic geology and geological evolution of the west Musgrave Region, central Australia (vol 27, pg 64, 2015). *Gondwana Research* 28, 1255.

Howard KE, Hand M, Barovich KM, Payne JL, Cutts KA and Belousova EA (2011) U–Pb zircon, zircon Hf and whole-rock Sm–Nd isotopic constraints on the evolution of Palaeoproterozoic rocks in the northern Gawler Craton. *Australian Journal of Earth Sciences* 58, 615–38.

Howard KE, Hand M, Barovich KM, Reid A, Wade BP and Belousova EA (2009) Detrital zircon ages: improving interpretation via Nd and Hf isotopic data. *Chemical Geology* 262, 277–92.

Iaccheri LM (2019) Composite basement along the southern margin of the North Australian Craton: evidence from in-situ zircon U-Pb-O-Hf and whole-rock Nd isotopic compositions. *Lithos* 324–325, 733–46.

Iaccheri LM and Kemp AIS (2018) Detrital zircon age, oxygen and hafnium isotope systematics record rigid continents after 2.5 Ga. *Gondwana Research* 57, 90–118.

Jackson MJ, Sweet IP, Page RW and Bradshaw BE (1999) The South Nicholson and Roper Groups: evidence for the early Mesoproterozoic Roper Superbasin. Integrated basin analysis of the Isa Superbasin using seismic, well-log, and geopotential data: an evaluation of the economic potential of the Northern Lawn Hill Platform. *Australian Geological Survey Organisation Record* 19.

Jackson MJ, Sweet IP and Powell TG (1988) Studies on petroleum geology and geochemistry, middle Proterozoic, McArthur Basin Northern Australia I: petroleum potential. *APPEA Journal* 28, 283–302.

Jackson SE, Pearson NJ, Griffin WL and Belousova EA (2004) The application of laser ablation-inductively coupled plasma-mass spectrometry to in-situ U/Pb zircon geochronology. *Chemical Geology* **211**, 47–69.

Javaux EJ, Knoll AH and Walter MR (2001) Morphological and ecological complexity in early eukaryotic ecosystems. *Nature* **412**, 66–9.

Johnson SP, Thorne AM, Tyler IM, Korsch RJ, Kennett BLN, Cutten HN, Goodwin J, Blay O, Blewett RS, Joly A, Dentith MC, Aitken ARA, Holzschuh J, Salmon M, Reading A, Heinson G, Boren G, Ross J, Costelloe RD and Fomin T (2013) Crustal architecture of the Capricorn Orogen, Western Australia and associated metallogeny. *Australian Journal of Earth Sciences* **60**, 681–705.

Kirkland CL, Smithies RH and Spaggiari CV (2015) Foreign contemporaries: unravelling disparate isotopic signatures from Mesoproterozoic Central and Western Australia. *Precambrian Research* **265**, 218–31.

Kirscher U, Mitchell R, Liu Y, Li ZX, Cox GM, Nordsvan A, Wang C and Pisarevsky S (2018) Long lived supercontinent Nuna – updated paleomagnetic constraints from Australia. American Geophysical Union (AGU) Fall Meeting, Washington, DC, abstract GP21B-0647.

Kositcin N, Beyer EE and Whelan JA (2014a) Summary of results. Joint NTGS–GA SHRIMP geochronology project: Arunta Region, July 2013–June 2014. *Northern Territory Geological Survey, Record* 2014-008.

Kositcin N, Beyer EE, Whelan JA, Close DF, Hallett L and Dunkley DJ (2013a) Summary of results. Joint NTGS–GA geochronology project: Arunta Region, Ngalia Basin, Tanami Region and Murphy Province, July 2011–June 2012. *Northern Territory Geological Survey, Record* 2013-004.

Kositcin N and Carson C 2017. New SHRIMP U-Pb zircon ages from the Birrindudu and Victoria basins, Northern Territory: July 2016–June 2017. *Geoscience Australia Record* 2017/16.

Kositcin N and Carson CJ (2019) New SHRIMP U-Pb zircon ages from the South Nicholson and Carrara Range regions, Northern Territory: July 2017–June 2018. *Geoscience Australia Record* 2019/09.

Kositcin N, Carson CJ, Hollis JA, Glass LM, Close DF, Whelan JA, Webb G and Donnellan N (2013b) Summary of results. Joint NTGS–GA geochronology project: Arunta Region, Davenport Province and Pine Creek Orogen July 2009–June 2011. *Northern Territory Geological Survey, Record* 2012-008.

Kositcin N, Champion DC and Huston DL (2009) Geodynamic synthesis of the North Queensland Region and implications for metallogeny. *Geoscience Australia Record* **30**, 1–196.

Kositcin N, Reno BL and Whelan JA (2015) Summary of results. Joint NTGS–GA geochronology project: Arunta Region, July 2014–June 2015. *Northern Territory Geological Survey, Record* 2015-007.

Kositcin N, Whelan JA, Hallett L and Beyer EE (2014b) Summary of results. Joint NTGS–GA geochronology project: Amadeus Basin, Arunta Region and Murphy Province, July 2012–June 2013. *Northern Territory Geological Survey, Record* 2014-005.

Kromkhun K, Foden J, Hore S and Baines G (2013) Geochronology and Hf isotopes of the bimodal mafic-felsic high heat producing igneous suite from Mt Painter Province, South Australia. *Gondwana Research* **24**, 1067–79.

Li ZX and Evans DAD (2011) Late Neoproterozoic 40 degrees intraplate rotation within Australia allows for a tighter-fitting and longer-lasting Rodinia. *Geology* **39**, 39–42.

Lyons TW, Reinhard CT and Planavsky NJ (2014) The rise of oxygen in Earth's early ocean and atmosphere. *Nature* **506**, 307–15.

Morrissey LJ, Barovich KM, Hand M, Howard KE and Payne JL 2019. Magmatism and metamorphism at ca. 1.45 Ga in the northern Gawler Craton: the Australian record of rifting within Nuna (Columbia). *Geoscience Frontiers* **10**, 175–94.

Morrissey LJ, Payne JL, Hand M, Clark C, Taylor R, Kirkland CL and Kylander-Clark A (2017) Linking the Windmill Islands, east Antarctica and the Albany-Fraser Orogen: insights from U-Pb zircon geochronology and Hf isotopes. *Precambrian Research* **293**, 131–49.

Mukherjee I and Large RR (2016) Pyrite trace element chemistry of the Velkerri Formation, Roper Group, McArthur Basin: evidence for atmospheric oxygenation during the Boring Billion. *Precambrian Research* **281**, 13–26.

Mukherjee I, Large RR, Bull S, Gregory DG, Stepanov AS, Avila J, Ireland TR and Corkrey R (2019) Pyrite trace-element and sulfur isotope geochemistry of paleo-mesoproterozoic McArthur Basin: proxy for oxidative weathering. *American Mineralogist* **104**, 1256–72.

Mukherjee I, Large RR, Corkrey R and Danyushevsky LV (2018) The Boring Billion, a slingshot for Complex Life on Earth. *Scientific Reports* **8**.

Munson TJ (2016) Sedimentary characterisation of the Wilton package, greater McArthur Basin. Northern Territory. *Northern Territory Geological Survey, Record* 2016-003.

Munson TJ, Thompson JM, Zhukova I, Meffre S, Beyer EE, Woodhead JD and Whelan JA (2018) Summary of results. NTGS laser ablation ICP-MS U–Pb and Lu–Hf geochronology project: Roper Group and overlying ungrouped units (McArthur Basin), Renner Group (Tomkinson Province), Tijunna Group (Birrindudu Basin). *Northern Territory Geological Survey, Record* 2018-007.

Murgulov V, Beyer E, Griffin WL, O'Reilly SY, Walters SG and Stephens D (2007) Crustal evolution in the Georgetown Inlier, North Queensland, Australia: a detrital zircon grain study. *Chemical Geology* **245**, 198–218.

Nebel O, Nebel-Jacobsen Y, Mezger K and Berndt J (2007) Initial Hf isotope compositions in magmatic zircon from early Proterozoic rocks from the Gawler Craton, Australia: a test for zircon model ages. *Chemical Geology* **241**, 23–37.

Neumann NL, Gibson GM and Southgate PN (2009) New SHRIMP age constraints on the timing and duration of magmatism and sedimentation in the Mary Kathleen Fold Belt, Mt Isa Inlier, Australia. *Australian Journal of Earth Sciences* **56**, 965–83.

Neumann NL and Kositcin N (2011) New SHRIMP U-Pb zircon ages from north Queensland, 2007–2010. *Geoscience Australia, Record* 2011/38, 1-82.

Neumann NL, Southgate PN, Gibson GM and McIntyre A (2006) New SHRIMP geochronology for the Western Fold Belt of the Mt Isa Inlier: developing a 1800-1650 Ma event framework. *Australian Journal of Earth Sciences* **53**, 1023–39.

Nordsvan AR, Collins WJ, Li ZX, Spencer CJ, Pourteau A, Withnall IW, Betts PG and Volante S (2018) Laurentian crust in northeast Australia: implications for the assembly of the supercontinent Nuna. *Geology* **46**, 251–54.

Nordsvan AR, Kirscher U, Kirkland CL, Barham M and Brennan DT (2020) Resampling (detrital) zircon age distributions for accurate multidimensional scaling solutions. *Earth Scivence Reviews* **204**, 103149.

Patchett PJ, Kouvo O, Hedge CE and Tatsumoto M (1982) Evolution of continental crust and mantle heterogeneity: evidence from Hf isotopes. *Contributions to Mineralogy and Petrology* **78**, 279–97.

Paton C, Hellstrom J, Paul B, Woodhead J and Hergt J (2011) Iolite: freeware for the visualisation and processing of mass spectrometric data. *Journal of Analytical Atomic Spectrometry* **26**, 2508–18.

Payne JL, Hand M, Barovich KM, Reid A and Evans DAD (2009) Correlations and reconstruction models for the 2500-1500 Ma evolution of the Mawson Continent. In Palaeoproterozoic Supercontinents and Global Evolution (ed. SM Reddy), pp. 319–55. Geological Society of London, Special Publication no. 323.

Payne JL, Pearson NJ, Grant KJ and Halverson GP (2013) Reassessment of relative oxide formation rates and molecular interferences on in situ lutetium-hafnium analysis with laser ablation MC-ICP-MS. *Journal of Analytical Atomic Spectrometry* **28**, 1068–79.

Planavsky NJ, Reinhard CT, Wang X, Thomson D, McGoldrick P, Rainbird RH, Johnson T, Fischer WW and Lyons TW (2014) Earth history. Low mid-Proterozoic atmospheric oxygen levels and the delayed rise of animals. *Science* **346**, 635–8.

Rawlings DJ (1999) Stratigraphic resolution of a multiphase intracratonic basin system: the McArthur Basin, northern Australia. *Australian Journal of Earth Sciences* **46**, 703–23.

Reid A, Hand M, Jagodzinski E, Kelsey D and Pearson N (2008) Palaeoproterozoic orogenesis in the southeastern Gawler Craton, South Australia. *Australian Journal of Earth Sciences* **55**, 449–71.

Reid AJ, Jagodzinski EA, Armit RJ, Dutch RA, Kirkland CL, Betts PG and Schaefer BF (2014) U-Pb and Hf isotopic evidence for Neoarchaean and Palaeoproterozoic basement in the buried northern Gawler Craton, South Australia. *Precambrian Research* **250**, 127–42.

Reid AJ, Jagodzinski EA, Wade CE, Payne JL and Jourdan F (2017) Recognition of c. 1780Ma magmatism and metamorphism in the buried northeastern Gawler Craton: correlations with events of the Aileron Province. *Precambrian Research* **302**, 198–220.

Reid AJ, Pawley MJ, Wade C, Jagodzinski EA, Dutch RA and Armstrong R (2020) Resolving tectonic settings of ancient magmatic suites using structural, geochemical and isotopic constraints: the example of the St Peter Suite, southern Australia. *Australian Journal of Earth Sciences* **67**, 31–58.

Reid AJ and Payne JL (2017) Magmatic zircon Lu–Hf isotopic record of juvenile addition and crustal reworking in the Gawler Craton, Australia. *Lithos* **292–293**, 294–306.

Reinhard CT, Planavsky NJ, Robbins LJ, Partin CA, Gill BC, Lalonde SV, Bekker A, Konhauser KO and Lyons TW (2013) Proterozoic ocean redox and biogeochemical stasis. *Proceedings of the National Academy of Sciences of the United States of America* **110**, 5357–62.

Scherer E, Münker C and Mezger K (2001) Calibration of the lutetium–hafnium clock. *Science* **293**, 683–87.

Sharman GR, Sharman JP and Sylvester Z (2018) detritalPy: A Python-based toolset for visualizing and analysing detrital geo-thermochronologic data. *The Depositional Record* **4**, 202–15.

Shen Y, Knoll AH and Walter MR (2003) Evidence for low sulphate and anoxia in a mid-Proterozoic marine basin. *Nature* **423**, 632–5.

Sheridan M, Johns DR, Johnson HD and Menpes S (2018) The stratigraphic architecture, distribution and hydrocarbon potential of the organic-rich Kyalla and Velkerri shales of the Upper Roper Group (McArthur Basin). *The APPEA Journal* **58**, 858–64.

Sláma J, Kosler J, Condon DJ, Crowley JL, Gerdes A, Hanchar JM, Horstwood MSA, Morris GA, Nasdala L, Norberg N, Schaltegger U, Schoene B, Tubrett MN and Whitehouse MJ (2008) Plesovice zircon – a new natural reference material for U-Pb and Hf isotopic microanalysis. *Chemical Geology* **249**, 1–35.

Spaggiari CV, Kirkland CL, Smithies RH, Wingate MTD and Belousova EA (2015) Transformation of an Archean craton margin during Proterozoic basin formation and magmatism: the Albany-Fraser Orogen, Western Australia. *Precambrian Research* **266**, 440–66.

Sperling EA, Rooney AD, Hays L, Sergeev VN, Vorob'eva NG, Sergeeva ND, Selby D, Johnston DT and Knoll AH (2014) Redox heterogeneity of subsurface waters in the Mesoproterozoic ocean. *Geobiology* **12**, 373–86.

Spikings RA, Foster DA, Kohn BP and O'Sullivan PB (2001) Late Neoproterozoic to Holocene thermal history of the Precambrian Georgetown Inlier, northeast Australia. *Australian Journal of Earth Sciences* **48**, 9–24.

Tang D, Shi X, Wang X and Jiang G (2016) Extremely low oxygen concentration in mid-Proterozoic shallow seawaters. *Precambrian Research* **276**, 145–157. doi: 10.1016/j.precamres.2016.02.005

Vermeesch P (2004) How many grains are needed for a provenance study? *Earth and Planetary Science Letters* **224**, 441–51.

Vermeesch, P (2013) Multi-sample comparison of detrital age distributions. *Chemical Geology* **341**, 140–6.

Vermeesch P (2018) IsoplotR: a free and open toolbox for geochronology. *Geoscience Frontiers* **9**, 1479–93.

Wade CE, Reid AJ, Wingate MTD, Jagodzinski EA and Barovich K (2012) Geochemistry and geochronology of the c. 1585Ma Benagerie Volcanic Suite, southern Australia: relationship to the Gawler Range Volcanics and implications for the petrogenesis of a Mesoproterozoic silicic large igneous province. *Precambrian Research* **206–207**, 17–35.

Wiedenbeck M, Alle P, Corfu F, Griffin WL, Meier M, Oberli F, Quadt AV, Roddick JC and Spiegel W (1995) Three natural zircon standards for U-Th-Pb, Lu-Hf, trace element and REE analyses. *Geostandards Newsletter* **19**, 1–23.

Williams B (2019) Definition of the Beetaloo Sub-basin. *Northern Territory Geological Survey, Record* 2019-015.

Withnall IW and Hutton LJ (2013) North Australian Craton. In *Geology of Queensland* (ed PA Jell), pp. 23–112. Brisbane: Geological Survey of Queensland.

Woodhead JD and Hergt JM (2005) A preliminary appraisal of seven natural zircon reference materials for in situ Hf isotope determination. *Geostandards and Geoanalytical Research* **29**, 183–95.

Woodhead JD, Hergt JM, Shelley M, Eggins S and Kemp R (2004) Zircon Hf-isotope analysis with an Excimer laser, depth profiling, ablation of complex geometries, and concomitant age estimation. *Chemical Geology* **209**, 121–35.

Worden KE, Carson CJ, Close DF, Donnellan N and Scrimgeour IR (2008) Summary of results. Joint NTGS-GA geochronology project: Tanami Region, Arunta Region, Pine Creek Orogen and Halls Creek January 2005–March 2007. *Northern Territory Geological Survey, Record* 2008-003.

Worden KE, Claoué-Long JC and Scrimgeour IR (2006a) Summary of results. Joint NTGS-GA geochronology project: Pine Creek Orogen, Tanami Region, Arunta Region and Amadeus Basin, July–December 2004. *Northern Territory Geological Survey, Record* 2006-006.

Worden KE, Claoué-Long JC, Scrimgeour IR and Doyle N (2006b) Summary of results. Joint NTGS-GA geochronology project: Pine Creek Orogen and Arunta Region, January–June 2004. *Northern Territory Geological Survey, Record* 2006-005.

Yang B, Collins AS, Blades ML, Capogreco N, Payne JL, Munson TJ, Cox GM and Glorie S (2019) Middle-late Mesoproterozoic tectonic geography of the North Australia Craton: U-Pb and Hf isotopes of detrital zircon grains in the Beetaloo Sub-basin, Northern Territory, Australia. *Journal of the Geological Society* **176**, 771–84.

Yang B, Collins AS, Cox GM, Jarrett AJM, Denyszyn S, Blades ML, Farkaš Y and Glorie S (2020) Using Mesoproterozoic sedimentary geochemistry to reconstruct basin tectonic geography and link organic carbon productivity to nutrient flux from a Northern Australian large igneous province. *Basin Research* **32**, 1734–1750. doi: 10.1111/bre.12450

Yang B, Smith TM, Collins AS, Munson TJ, Schoemaker B, Nicholls D, Cox G, Farkas J and Glorie S (2018) Spatial and temporal variation in detrital zircon age provenance of the hydrocarbon-bearing upper Roper Group, Beetaloo Sub-basin, Northern Territory, Australia. *Precambrian Research* **304**, 140–55.

Zhang K, Zhu XK, Wood RA, Shi Y, Gao ZF and Poulton SW 2018. Oxygenation of the Mesoproterozoic ocean and the evolution of complex eukaryotes. *Nature Geoscience* **11**, 345.

Zhu S, Zhu M, Knoll AH, Yin Z, Zhao F, Sun S, Qu Y, Shi M and Liu H (2016) Decimetre-scale multicellular eukaryotes from the 1.56-billion-year-old Gaoyuzhuang Formation in North China. *Nature Communications* **7**, 11500.